Master in Chemical Engineering

Development of ZnO anodes for high capacity batteries

Master´s Thesis

by

Tânia Isabel Moreira Gonçalves

Developed in the course unit of Dissertation

Performed in

DLR – Institute of Engineering Thermodynamics

Supervisor at DLR: **Eng. Natalia Cañas, Dr. Dong-Won Park**

Supervisor at FEUP: **Prof. Adélio Mendes**

Universidade do Porto

Faculdade de Engenharia

FEUP

Department of Chemical Engineering

March 2015

Acknowledgments

I am deeply grateful for the opportunity of working on this topic which contributes to the development of a new set in lithium-ion batteries. My work was never done before in DLR - Institute of Technical Thermodynamics, it is very recent in the world and its future application is for electric vehicles and hybrid electric vehicles. Moreover, the development of ZnO anodes for high capacity batteries made me acquire skills and practice methods that I will take for life. Thank you to everyone who made this possible and enjoyable.

I am very grateful to my professor and supervisor Adélio Mendes for creating this partnership between FEUP and DLR. Thank you for the supervision of my work, brilliance and great knowledge shared with me. Thank you to my professor Miguel Madeira who is responsible for the Erasmus Internship Programm for accepting me to do the master thesis in DLR. Moreover, I would like to express my gratitude to all the professors who taught me and transmitted their knowledge and experience during my studies because that became possible the achievement of this point.

Thank you to Norbert Wagner for accepting my application to do my master thesis in DLR because this experience made me learn by doing and searching while having the supervision of great supervisors. I am grateful to have received great supervisors who shared with me their knowledge, brilliance, way of thinking and doing: thank you so much to Natalia Cañas, my direct supervisor at DLR, for the continuous support in all my tasks, good work experience and knowledge shared because this made possible everything; thank you so much to Dong-Won Park for the experimental work, availability in helping and sharing knowledge with me.

Thank you for the good environment at DLR with the colleagues who shared their knowledge and helped me in some way. Thank you to Werner Seybold for helping me pressing the anodes. Thank you to Thomas Oliver Freitag, Christopher Heim, Miriam Klein and Brigitta Pascucci for the helpful tips and sharing of experience. Thank you to everyone of the battery technology group who assisted to the presentation of my work.

I am grateful to all my friends at DLR: Srijeeta Sen, Sebastian Mal, Philipp Einsiedel, Daniel Gottsche, Thao and Ali for the friendship, company and good moments.

Thank you to my parents and whole family, to my friends in Germany and in Portugal, for their continuous company and joy on me.

Abstract

Zinc oxide (ZnO) is suitable as anode material for lithium-ion batteries due to the high capacity (987 $mAh.g^{-1}$) and electron mobility (>100 $cm^2\ V^{-1}\ s^{-1}$). Other advantages are the low cost material, abundant and environmentally safe. As a transition metal, ZnO provides solutions for the problems of volume expansion, like occurring in the silicon and tin anode.

Mechanical milled ZnO particles increased the surface area for improving the contact with lithium-ions and the conductive component. Among the synthetized electrodes, one hour mechanical milled ZnO provides the plank nano-structure of the active material which allows the highest capacity and slowest capacity fading during cycling. Electrodes fabricated from commercial powder (ZnOc, micro-size) and commercial suspension of ZnO Nanoparticles (ZnOsp, nano-size), exhibited capacity fading fast in the first cycles and low capacities.

Higher milling times provides higher levels of contamination with iron oxides, Fe_xO_y, which results in increase of contact resistance of the electrode with the lithium ions and increase of capacity fading in the first cycles. Pressing all electrodes enhances the capacity by increasing density and stability of electrode.

The most stable half-cell revealed ca. 450 mAh g^{-1} of reversible capacity at the 63^{th} cycle and Coulombic efficiency near 100 % during cycling. One hour of mechanical milling allows the lowest contamination with iron oxides and highest surface area contact of the active material ZnO. The pressed electrode in which the active material is synthetized in 1 h of mechanical milling time and results in the plank structure, presents the highest capacity, cyclability and durability.

Key-words Metal oxides, zinc oxide synthetized, high capacity lithium-ion battery

Sumário

O óxido de zinco é um elétrodo negativo preferível para as baterias de ião-lítio devido à elevada capacidade (987 mAh g^{-1}) e mobilidade eletrónica (>100 cm^2 $V^{-1}s^{-1}$). Como metal de transição oferece soluções para os problemas de expansão de volume dos elétrodos de silício e de estanho. ZnO é um anode promissor para as baterias de ião-lítio. É um material de baixo custo, abundante e livre de poluição para o ambiente.

A moagem mecânica reduziu o tamanho das partículas para o aumento da área da superfície de contato com os iões de lítio e o componente condutor. Entre os elétrodos sintetizados, uma hora de moagem mecânica de ZnO sintetizado originou a nano-estrutura em forma de prancha do material ativo o que correspondeu à mais elevada capacidade e mais lenta perda de capacidade durante os ciclos. Os eletrodos cujo material ativo proveio do pó comercial (ZnOc, tamanho micro) e suspensão comercial (ZnOsp, tamanho nano) exibiram rápida perda de capacidade nos primeiros ciclos e baixas capacidades.

Tempos mais elevados de moagem originam maiores níveis de contaminação com óxidos de ferro, Fe_xO_y, o que resulta no aumento da resistência do elétrodo ao contato com os iões de lítio e no aumento da perda de capacidade nos primeiros ciclos. A pressão de todos os elétrodos reforça a capacidade através do aumento da densidade e área de surperfície do material ativo.

A meia-célula ZnOs1 cujo material ativo foi moído durante 1 h, apresentou quase 450 mAh g^{-1} de capacidade reversível no 63º ciclo e eficiência de corrente estável em 100 % em quase todos ciclos. Uma hora de moagem mecânica de ZnO permite a menor contaminação com óxidos de ferro e a maior área de contato do material ativo. O elétrodo pressionado, cujo material ativo é sintetizado em 1 h de moagem mecânica e resulta em nano-estrutura prancha, apresenta a mais elevada capacidade, ciclabilidade e durabilidade.

Key-words Metais de transição, óxido de zinco sintetizado, baterias de ião-lítio de elevada capacidade

Declaration

Eu, Tânia Isabel Moreira Gonçalves declaro, sob compromisso de honra, que este trabalho é original e que todas as contribuições não originais foram devidamente referenciadas com identificação da fonte.

Contents

Glossary

List of abbreviations

CB	Carbon black
CMC	Carboxymethyl cellulose
EV	Electric vehicles
HEV	Hybrid electric vehicles
Li-ion	Lithium ion
OCV	Open Circuit Voltage
PLion	Polymer lithium-ion
SEI	Solid electrolyte interface
SEM	Scanning electron microscopy
SHE	Standard Hydrogen Electrode
XRD	X-ray diffraction
ZnOc	Zinc oxide powder commercial
ZnOs	Zinc oxide powder synthetized
ZnOsp	Zinc oxide commercial suspension

List of constants

α	Symmetry parameter of redox reactions
A	Arrhenius constant
E_a	Activation energy constant
F	Faraday constant: 96485 C mol-1
k	Kinetic constant
R	Gas constant: 8.314 $J.mo^{-1}K^{-1}$

List of symbols

$\Delta E°$	Cell potential in equilibrium (V)
ΔG_{eq}	Gibbs free energy in equilibrium ($J.mol^{-1}$)
a_i	Activity coefficient ($mol.dm^{-3}$)
C^*_{oxd}	Concentration of the oxidized specie ($mol.dm^{-3}$)
C_{oxd}	Concentration of the anode before oxidation ($mol.dm^{-3}$)
C_{red}	Concentration of the cathode before reduction ($mol.dm^{-3}$)
C^*_{red}	Concentration of the reduced specie ($mol.dm^{-3}$)
E	Potential (V)
D	Diffusional coefficient (m^2/s)
I	Current (A)
i	Current density ($A.cm^{-2}$)
i_0	Exchange of current density ($A.cm^{-2}$)
n	Number os electrons per mole (mol^{-1})
Q	Heat (J)

R	Resistance (Ω)
t	Time (s)
η	Over potential (V)

1 Introduction

1.1 High capacity lithium batteries

Worldwide there has been a demand for high capacity storage systems for vehicles and electronics. Batteries store electrical energy in the form of chemical energy released in the redox reactions that take place at the surface of the electrodes. Their fundamental characteristics must be facile materials availability, low maintenance, long life span, low chemical, acoustic and thermal emissions, and low carbon dioxide emissions due to the low oxidation temperatures.

The development of better batteries has been of great importance to the technology evolution and the consumption demand of an increasing world population. Figure 1 shows the volumetric energy density and specific energy for the most utilized batteries. Among these batteries, lithium batteries present the advantageous features of low self-discharge, high energy density, high specific energy, high voltage and charge retention due to the electrochemical and chemical proprieties of lithium. Lithium has the highest negative standard reduction potential of -3.04 V_{SHE} and it is suitable for mobile electrical systems due to the density of 0.54 g cm^{-3}. [1]

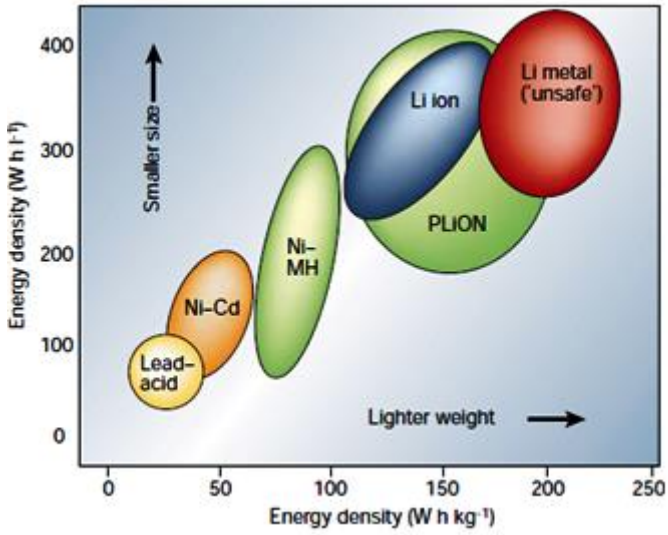

Figure 1- Variation of the volumetric energy density and the gravimetric energy density of common batteries and lithium batteries. [1]

Batteries consist of several cells connected in series or parallel to provide a required voltage therefore the battery is characterized by the proprieties of its smallest unit: the cell. The electrode with the highest negative standard reduction potential is the anode where oxidation occurs which, in case of discharge, is the negative electrode. The reduction reaction occurs in the cathode that is the positive electrode during discharge. The electrons circulate from the negative electrode to the positive electrode while the current circulates from the positive electrode to the negative electrode. Lithium has been utilized as anode due to its highest negative SHE in batteries that allow high capacity.

Capacity is the current discharged integral over time under a determined voltage. Lower discharge rates (*C rates*) correspond to higher capacities if the active centers of the electrodes are activated although for semiconductors such as zinc oxide it might be necessary to apply high current for electrode activation and occurrence of redox reactions. When the battery receives a charge of one ampere (1 A) passed one coulomb (1 C) of charge per second. As the C rate increases, the operating capacity decreases due to the ohmic drop. Low C rates correspond to low levels of current being discharged in a long period of time. Polarization accounts the electrical potential difference between the operating voltage and the operating voltage at an equilibrium state. During discharge the operation voltage is always lower than the electric potential in equilibrium.

Several electrodes materials have been defining the current applied for their performance and capacity storage. Polymer lithium-ion batteries (PLion) and lithium-ion batteries (Li-ion) have the highest capacities and smallest size that make them suitable for high capacity systems. However, lithium batteries have security problems as the lithium ion becomes unsafe under certain conditions therefore it is important to have knowledge of these problems.

For the development of high capacity batteries with lithium as anode the temperature range is 0 ºC to 100 °C and the voltage range of operation is 2 to 4 V. At higher values of energy storage, lithium metal reacts with the organic liquid electrolyte and during cycling there is an increase of surface area. At higher voltage occurs lithium plating and loss of capacity. The Coulombic efficiency lower than 100 % is due to the film deposited on its surface in every cycle that reduces the active surface area of the electrode. The capacity degradation increases for higher temperatures. As the temperature and pressure increases more than 100°C the separator melts, the Solid Electrolyte Interface (SEI) breaks down, inflammable gases and oxygen are released leading to explosions, fire and several security problems. Operating under 0 V or at negative temperatures also lead to electrodes breakdown and short circuit.

Besides these problems, lithium batteries are expensive. Therefore, finding materials abundant in nature, cheap that can deliver high capacities and have long durability and cyclability and

are environmentally free is fundamental to supply the demand of the worldwide energy consumption through high capacity reversible batteries.

1.1.1 The lithium-ion battery

The first reversible battery was made with lithium-metal as anode and titanium disulfide, TiS_2, as cathode by Exxon. The principle of operation was set in the utilization of chalcogenides which are high conductive, light and allow the lithium ions to be intercalated easily. This battery had a theoretical capacity of 239 mAh g^{-1} and long cycling. [1] However, it was not widely used due to the high volume expansion during recharge and explosion problems.

The concept of lithium-ion battery appeared with the utilization of a lithium alloy as anode which provides the solution for the dendrite growth of the previous battery. This increased in potential led to utilization of metal oxides as cathodes due to their ability of multi-layered intercalation coming from their various oxidation states. The following cathode utilized in lithium batteries was molibdeminum disulfide, MoS_2, though this material induces short circuit problems and overheating.

Oxides were developed using carbon as anode and $LiCoO_2$ as cathode which induces a cell voltage of 3.7 V, an irreversible capacity of 272 mAh g^{-1}, reversible capacity of 140 mAh g^{-1} and good cyclability. [2] Other batteries were developed utilizing metal oxides alloys with lithium as cathodes such as $LiMn_2O_4$ (148 mAh g^{-1}), which has problems of capacity retention, and $LiNiO_2$ (275 mAh g^{-1}) which as problems of capacity fading though these materials are cheaper. [3] Transition metal oxides electrodes when utilized as anodes operate a lower potential and higher capacity than when utilized as cathodes as it can be observed in Figure 2. They have a wide capacity range and limited cycling.

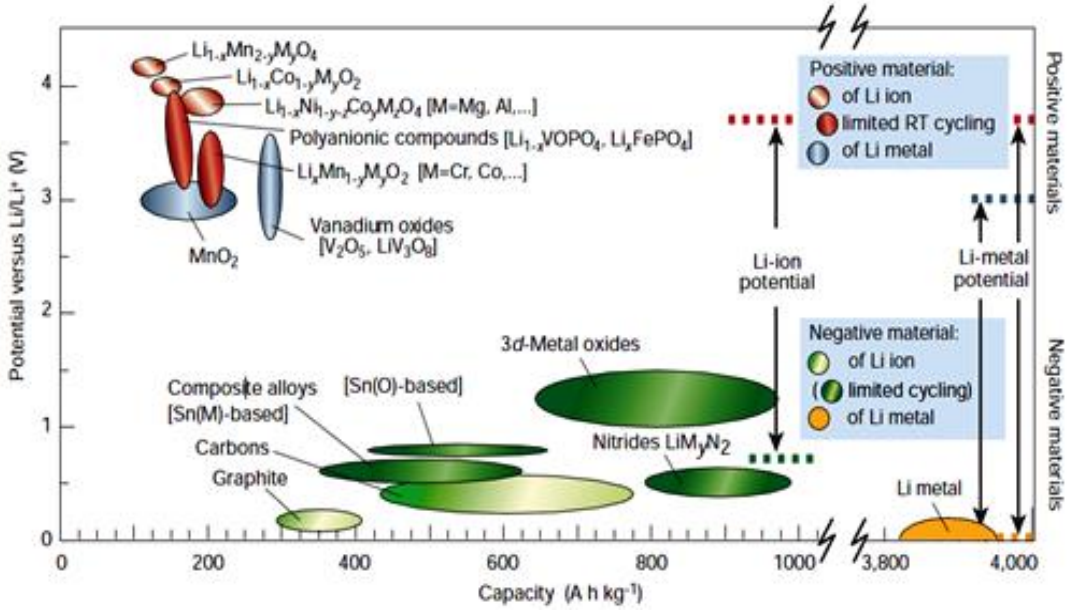

Figure 2 - Relation between capacity and potential for anodes comparing with lithium. [1]

Other attempts to produce higher capacity batteries are in utilizing anodes such as carbon and silicon. Carbon anode exhibits the reversible capacity 378 $mAh.g^{-1}$ and when added to other anode materials enhances the conductivity of the electrons but it has capacity fading during the irreversible capacity due to reduction of the electrolyte and consequent formation of the solid electrolyte surface (SEI).

Silicon anodes have the highest capacity among anodes (4200 mAh g^{-1}) although they present low capacity retention caused by 400 % of volume expansion during reversible processes, limiting cycling and capacity stability. This is due to electrode pulverization and breaking down of the solid electrolyte interface film which decreases the conductivity of the collector. [4]

Table 1 presents the capacity, volume change and relevant electrochemical characteristics for the electrodes presented. The alloy titanium oxide with lithium $Li_4Ti_5O_{12}$ has the lowest volume change, following by carbon, although its capacity is the lowest for the anodes presented. Lithium alloys in which elements such as Sn, Sb, Al and Mg are present have high volume changes.

Table 1 – Chemical and electrochemical characteristics of anodes in li-ion batteries. [5]

Materials	Li	C	$Li_4Ti_5O_{12}$	Si	Sn	Sb	Al	Mg
Density (g cm^{-3})	0.53	2.25	3.5	2.3	7.3	6.7	2.7	1.3
Lithiated phase	Li	LiC_6	$Li_7Ti_5O_{12}$	$Li_{4.4}Si$	$Li_{4.4}Sn$	Li_3Sb	LiAl	Li_3Mg
Capacity (mAh g^{-1})	3862	372	175	4200	994	660	993	3350
Volume change (%)	100	12	1	420	260	200	96	100
Potential vs Li (V)	0	0.05	1.6	0.4	0.6	0.9	0.3	0.1

The volume expansion comes from the discharge in the first cycle where there is incomplete dealloying. The lithium ions released into the anode, do not get back to the cathode during charge (alloying), causing loss of contact area between the active material and the lithium-ions and increase of internal resistance of electrode. This results in capacity fading fast in the first cycles, breakdown of the electrode and decrease of cyclability and durability of the battery.

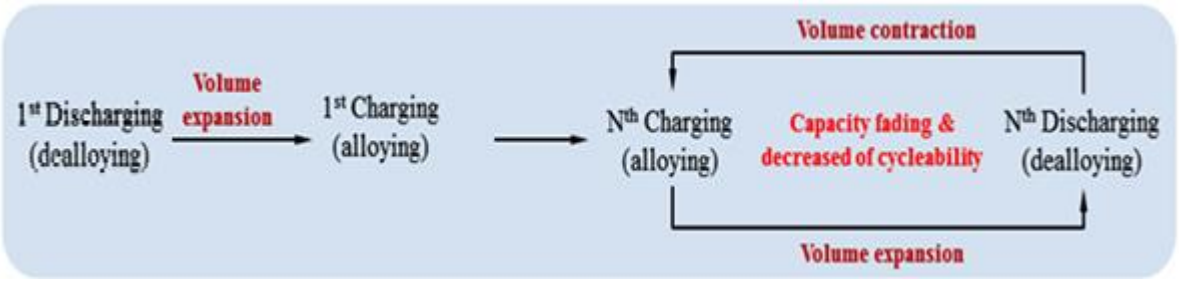

Figure 3 – Volume variations and impacts on cyclability and durability of lithium-ion batteries.

Lithium-sulfur batteries have presented high energy storage (2500 mWh g^{-1}) as well as theoretical capacity (1675 mA g^{-1}) but these batteries explode easily in a collision due to the reactivity of sulfur. There is large volume expansion during cycling and capacity fading due to dendrites and degradation processes. The low electronic conductivity of the cathode contributes to the degradation of the battery during the first cycle. During cycling the reactivity with the organic electrolyte produces polysulfides and results in low Coulombic efficiencies. [6]

Lithium-air batteries store high capacities.This is due to utilization of lithium as anode and oxygen as cathode that provides reversible capacity of 3862 mA g^{-1}. Although the good cyclability of these batteries, lithium is very reactive with the smallest particles of water that can be present, resulting in facile short circuit. [7] This main problem compromises the lithium performance in the battery and sets new advancements in the lithium-ion battery.

1.1.2 Transition metals as anodes

Metal oxides promise higher capacity batteries due to the high reversible reactivity with lithium. They present themselves among pure elements or elements that form alloys with lithium, spinel and graphitized carbons in anode synthesis for safer lithium batteries. This main characteristic is due to the valence electrons occupying the orbital corresponding to the highest energy *s* of the latest layer and when this orbital is full, the valence electrons occupy the orbital d of the previous layer which has lower energy *d* and higher electrical instability. This orbital allow high values of excitation energy for the valence electrons, easy releasement of the electrons and formation of many oxidations states for the same element.

Metal oxides are chemical components that favor the formation of different alloys with lithium through redox reactions on the surface of the electrodes. They have higher capacity than carbon anodes (see Figure 3) mainly due to the electrons that are released during discharge coming from the orbital *d*, which allows high electrical conductivity and many oxidation states.

Challenges to overcome are in finding ways of compensating the potential difference and the instability during cycling, low conductivity and fast capacity fading in the first cycles.

The first metal oxides applied as anodes in lithium-ion rechargeable batteries were SnO and Sn_2O by a patent of Fuji Photo Film Co. Ltd [8]. In 1999 Hong et al described the alloying reaction of metal oxides, MO as a two-step reaction. [9] The first irreversible reaction (1) accounts for the greater loss of oxide and increase of volume because the lithium oxide and metal *M* are produced. In the second reaction (2) the metal reacts with lithium to form a new alloy and reversible capacity.

$$(2\,y - x)\,Li + Li_xMO_y \rightarrow y\,Li_2O + M\ (x \geqslant 0)\ (1)$$

$$xLi + M + e \leftrightarrow Li_xM\ (2)$$

Hong et al [9] found out that following oxide: CuO, Fe_2O_3, In_2O_3, PbO, Sb_2O_3, ZnO, SnO and SnO_2 did not reach higher reversible capacities due to the large capacity loss during the first discharge which reveals kinetic limitations. [9] Zinc oxide was first tested as anode material by Hong et al [9] with a Columbic efficiency of 61 % and a reversible capacity far away from the reported value of 987 mAh g^{-1}. In the first cycle a discharge capacity of 650 mAh g^{-1} was obtained, while in the 13^{th} cycle, 250 mAh g^{-1}. It was found out the particle size of 100 nm obtained in mechanical milling was important for the highest columbic efficiency of the metal oxides studied.

Recently, several attempts have been applied in using SnO_2 as anode material, which has reversible capacity of 1494 mAh g^{-1} and form composites that have lower volume expansion and therefore, better electrochemical performance. [10] Silicon has been utilized in lithium-ion batteries due to the higher capacity of 4200 mAh g^{-1}; however, problems with huge volume expansion, low conductivity and diffusion has led to the addition of ZnO to Si anode to form a composite with less capacity degradation and improved battery performance. [11] [12]

Among all metal oxides, ZnO has multiple storage of lithium ions during the alloying with lithium and it allows higher capacity retention due to high electronic conductivity and stable porosity nanostructure with the conductive material such as carbon black. ZnO kinetics limitations depend on the chemical synthesis methods and materials as well as the fabrication of the anode electrode. In this context, zinc oxide presents as alternative anode material for lithium-ion batteries that can increase the capacity of the latest rechargeable batteries.

1.2 Electrochemical characteristics required for reversible batteries

The required characteristics of a reversible battery are related with high power and high capacity which depends the concentration gradients of reactants and on the rate they reach the electrode surface. The cell design must have the suitable conditions for the maximization of this rate. Furthermore, the diffusional pathway for the transport of ions from the anode to the cathode through the electrolyte dictates the convenient transfer of electrons through the external circuit load. This load is a conductive path that allows the continuous electron flux to produce high electromotive force and current. The anode must have low voltage in Open Circuit Voltage (OCV). The anode as well as the cathode must be conductive, non-toxic and low-cost.

For lithium-ion batteries, the electrolyte must be a ion conductive, electrical isolating and protective of side-reactions by formation of the SEI on the interface with the electrodes. The resistance increases with increasing current density. When the electrolyte is in excess, cations are surrounded by an excess of ions negatively charged, which causes a drop in the free energy of these cations leading to an decrease of the activity coefficient. This results in an increase of the energy necessary for their movement and transportation across the electrolyte. Short circuit happens due to the flux of electrons that move from the anode to the cathode along the external load. As there is no movement of ions, ions stay in large amounts at the cathode, leading to high values of current produced in a very short period of time. Eventually if the electrolyte is present in high quantities, that it becomes impossible the cations to move across the electrolyte, they become accumulated at the surface of the anode. This occurrence makes impossible further oxidation of the anode. Therefore no voltage is produced as well as current.

An approach to have efficient lithium-ion batteries is in finding ways of dismissing the losses. This begins the selection of the operating potential near the value of the potential at equilibrium where there is no flux of ions. During the discharge this operating potential is lower than the state of equilibrium potential. This overpotential is due to polarization. This is the state which corresponds to the maximum work possible to produce and is called reversible work and corresponds to the Gibbs free energy, ΔG (J mol^{-1}). As present in the equation (3) the Gibbs free energy in equilibrium is related with the cell potential and it is determined by the product of cell potential, ΔE^o (V), number of electrons released per mol of reagent, n (mol^{-1}), and the Faraday constant, F, (96485 C mol^{-1}).

$$\Delta G\ eq = -\Delta E^o\ \ n\,F \tag{3}$$

The flux of electrons per second is $1/F$ which corresponds to $1\ A$ (charge flux of 1 C s^{-1}). This equilibrium potential is given by the Nernst equation (4) which depends on the activities of materials as well as number of electrons transferred. The gas constant R is 8.314 J mol^{-1} K^{-1},

the activity coefficients a_i of all species in the global reaction of the cell and υ_i is their respective stoichiometric coefficient.

$$\Delta E = E_{eq\ positive\ electrode} - E_{eq\ negative\ electrode} = \Delta E^0 - \frac{R\,T}{n\,F} \ln \Pi\ (a_i)^{\upsilon_i} \quad (4)$$

The Gibbs free energy depends on the kinetics of the chemical reactions therefore at equilibrium state when the cell reaches the initial conditions of constant temperature and constant pressure; this corresponds to the maximum possible work. The existence of a suitable catalyst is important because this increases the kinetics of molecules which decreases the amount of activation energy, E_a, for the reactions to take place by increasing the temperature *T* at which the reactions take place accordingly to the Arrhenius's law (5) where *A* is a constant dependent on the rate reaction *k*.

$$k = A\ e^{-\left(\frac{E_a}{R\,T}\right)} \quad (5)$$

This must be studied as the heat *Q* depends on the current *I* accordingly to Joule's law (6) where the current I varies with the time *t*.

$$Q = R \int_{t_1}^{t_2} I^2\, dt \quad (6)$$

Low reaction rates *K* lead to low levels of current and power produced. Low temperatures indicates low internal resistance due to low reactivity of reactants accordingly to Arrhenius equation which results in discharging at lower voltage, lower resistance and higher capacity. The electrochemistry in the cells, it is fundamental to observe the current density *i* ($A.cm^{-2}$) and the over potential η (V) profiles given by the Butler-Volmer equation (7) where:

$$i = i_0 \left\{ \frac{C_{red}}{C^*_{red}}\ e^{\left[\frac{\alpha_{Oxd}\,F\,(E-E_{eq})}{R\,T}\right]} - \frac{C_{Oxd}}{C^*_{Oxd}}\, e^{\left[\frac{\alpha_{Red}\,F\,(E-E_{eq})}{R\,T}\right]} \right\} \quad (7)$$

$$\eta = E - E_{eq} \quad (8)$$

When the over potential η is zero that corresponds to the equilibrium, the exchange current density i_0 is given by equation (9):

$$i = |i^+| = |i^-| \quad (9)$$

Where $i^+ = i_0\, e^{(1-\alpha_{Red})\frac{n\,F}{R\,T}}$ and $i^- = -i_0\, e^{-\alpha_{Oxd}\frac{n\,F}{R\,T}}$ corresponds to the anodic part and cathodic part of the Butler-Volmer equation respectively. In the cell operation the symmetrical parameter α defines which redox reaction is favored (0 < α < 1). [13]

The first irreversible loss is the activation over potential. It is related with the electrons released and sets the scan rate of potential change in electron transfer at lower currents. The charge transfer through the phase boundary depends on proprieties of reactants, electrolyte and electrode. By analysis of the current behavior between the cell range potential at a constant rate of voltage, which corresponds to the cyclic voltammetry is possible to obtain the information on the reversible electrochemical reactions. The activation over potential determines the rate transfer of electrons that happens until a certain phase boundary, sets the potential at low currents and depends on the nature of the species involved in reaction, proprieties of electrolyte and proprieties of electrode. In order to increase the speed of the redox reactions it is necessary to increase the electrode surface area because this allows more area where the reactions take place or utilize a catalyst. It is related with the amount of activation energy for the redox reactions to occur. An increase on the surface roughness yields to higher speed redox reactions. The larger the drop in potential at neutral currents, the higher is the activation overpotential. [13] [14]

The concentration over potential is the potential variations due diffusional variations. It represents delays in reaching steady conditions due to the use or production of materials related with the concentration of the species at the surface of the electrodes. Therefore is influenced by pressure gradients, materials porosity such as diffusion by the gas layer, gas or liquid influences and the permeability of membrane or electrolyte such as flux of ions. If the current is kept constant while the voltage is decreasing then the over potential is mainly due to diffusional processes. The typical graphic curve that represents the variation of potential across the current has an exponential behavior in a large range of currents which is explained by the Butler-Volmer equation (6). At higher potentials the limitations in speed current are due to diffusional processes. However the rate of electron transfer is higher than the variation of reactants transfer at the surface of electrodes, which corresponds to the decrease of concentration of reactants at the electrodes surface and exchange of current density near to zero. The diffusion coefficient of lithium ions across the electrolyte is given by *D* through the

Fick's law (9) which provides knowledge on how the concentrarion of lithium-ions c in the electrolyte, with a *x* path length, varies with time *t*.

$$\frac{\partial \mathrm{c}}{\partial \mathrm{t}} = -D \frac{\partial^2 \mathrm{c}}{\partial \mathrm{x}} \quad (10)$$

The IR drop is related with the voltage drop across the electrolyte given by Ohm´s law (10) where *R* is the resistance, *E* is the voltage and *I* is the current. There must be a driving force that brings electrons and protons to their respective electrode. This causes not only a voltage drop that affects the efficiency reaction but also sets a limit on the reaction rate due to the diffusional rate. [14]

$$R = E/I \quad (11)$$

The internal resistance must be measured with an impedance meter on the Ohm Test Programme. The voltage should remain constant along cycling. The manufacturing of the cell components such as the electrodes and supporters should be controlled in order to have the less presence of impurities that can contaminate the cell along the cycling whereas parameters such as temperature are not kept precisely constant. Controlling the charging time by discharging the battery at a lower percentage of its full capacity in order to not overcharge and increase the cell temperature is important for the cell not suffer from stress and perform naturally.

The approach to find better operation proprieties is related with the study the degradation processes as well as knowing the chemical reactions occurring and by-products, developing new technologies for high efficient synthesis processes as well as materials with higher specific energy which are abundant in nature, have low cost, are environmental friendly, can operate at a wide range of temperatures, have higher theoretical and operational capacity, long cycle life, have intrinsic systems of protection against overcharge, delivering the full capacity and operating at normal voltages even after many discharging and charging cycles, tolerated to overcharge, no volume variations. The conductive mean such as membrane or electrolyte must have a thin thickness for an easy flow of ions or be in a suitable quantity. The distance between electrodes and the right amount of electrolyte in order to not occur side reactions and all components must support corrosion.

After a battery has been discharged and charge many times, the tendency to self-discharge increases due to hysteresis. The pressure inside the battery is higher after cycling which leads to the swelling of electrodes against the separator. Metallic dendrites which are the result of crystalline structure are formed due to the quantity of current produced. New electrodes and batteries have to be constructed to overcome these problems.

1.3 Background and project presentation

Zinc oxide is a promising anode material for high capacity batteries mainly to the high capacity of 987 mAh g^{-1}. It is a better alternative to the carbon anodes which offer the low capacity of 372 $mAhg^{-1}$. It has lower volume expansion than silicon anodes and does not provide occurrence of side-reactions as lithium-sulfur where there is formation of polysulfide. It is a low cost material, abundant in nature, easy to prepare, chemical stable and nonhazardous. However, low capacity retention and an incomplete understanding of degradation problems are the main drawbacks of this electrode.

This work focuses on the synthesis of ZnO and its comparison with the ZnO-anodes produced with commercial powder and suspension. The mechanical process for the electrode synthesis was the mechanical ball milling and the tape casting (doctor blade) was prepared for the electrode fabrication. It was also observed the influence of pressing the electrodes before the Swagelok Cell assembling.

Moreover, preparation of ZnO electrodes and electrochemical characterization of the electrode (vs. Li) were performed to the Swagelok cell. X-ray diffraction (XRD) and scanning electron microscopy (SEM) were used to characterize the morphological and structural changes after cycling. Furthermore, cyclic voltammetry and electrochemical cycling at different C rates were also investigated to characterize the behavior of different zinc oxide electrodes in the lithium-ion battery.

1.4 German Aerospace Center

The German Aerospace Center (DLR), Institute of Engineering Thermodynamics in Stuttgart is developing research and efficient energy storage technologies with high economical potential and low environment impact. This has been setting the energy storage market in Germany and contributing to the continuous development of German energy industries and society.

The department of Electrochemical Energy Technology has been impacting the transportation energy in Germany. One of its main topics is developing advanced lithium batteries, especially lithium-air and lithium-sulfur batteries for high capacity systems such as electric vehicles (EV),

hybrid vehicles (HEV), hydrogen storage systems and fuel cells technologies [15]. Analyzing batteries degradation processes and finding solutions to have higher efficiencies has led to the development of safer new electrodes.

For the first time at DLR, ZnO-anodes were synthetized, prepared and characterized in the context of this master thesis. Promising properties such as higher energy storage, low cost and maintenance, high Coulombic efficiency, rehabilitee, silence and environmentally safe, make ZnO an attractive anode material for high capacity batteries.

1.5 Contribution of the work

This work contributes to the research and production of high capacity batteries through finding a better method of synthetizing zinc oxide and providing knowledge on the transition metals as anodes in lithium batteries.

The aim is to investigate the electrode pulverization, volume expansion phenomena and capacity fading during the cycling.

The application of producing ZnO anodes for high capacity lithium batteries is for EV and HEV and mobile electric systems.

1.6 Thesis organization

The first chapter is the background of the batteries development with focus on high capacity batteries and lithium-ion batteries while relating the main electrochemical characteristics of

the electrodes. It is made an approach of how metal oxides are better electrodes and the discovery of zinc oxide as a new anode in the li-ion battery.

Chapter 2 is the state of art which presents the chemical and physical characteristics of ZnO as well as the procedures to its synthesis along with the electrochemistry of the zinc oxide in the lithium-ion battery namely: fundamental principles, chemical reactions and degradation behaviors.

In chapter 3, the experimental work, such as synthesis and preparation of the active materials through mechanical milling, fabrication of the ZnO electrodes through tape casting, the Swagelok half-cell battery assembling, battery cycling, XRD and SEM characterization.

Chapter 4 presents the results of this work for the different types of the electrodes: SEM pictures, XRD graphics, comparison between micro-size particles and nano-size particles electrodes, influence of milling time of synthetized electrodes, cyclic voltammetry, and comparison of pressed and non-pressed electrodes and electrochemical test of an electrode synthetized.

In the chapter 5 it is presented the conclusions of this work, acknowledgments and solutions for the future.

2 State of Art

2.1 Chemical and physical proprieties and applications of zinc oxide

Zinc oxide is a transition metal oxide which has been utilized in the rubber industry mostly, following by fields such as ceramics; chemical processing and electronics (see Figure 4). The wide range of applications includes pharmaceutics, coatings, pigments and agriculture. Worldwide 1.2 million tons of ZnO are produced per year. [16] It has the great advantage of being nonhazardous in the environment. At room temperature it is white and the crystal chemical structure is the wurzite. In the rubber industry zinc oxide activates sulphur vulcanization. It is also a catalyst in the steam reforming of methanol [17], production of hydrogen [18], production of biodiesel from soyabean [19] and removal of pollutants from waste water. [20] It is commonly used in alloys, paintings, coatings, oil additives, animal feed and fire retardants. It is a material of foundation and galvanization.

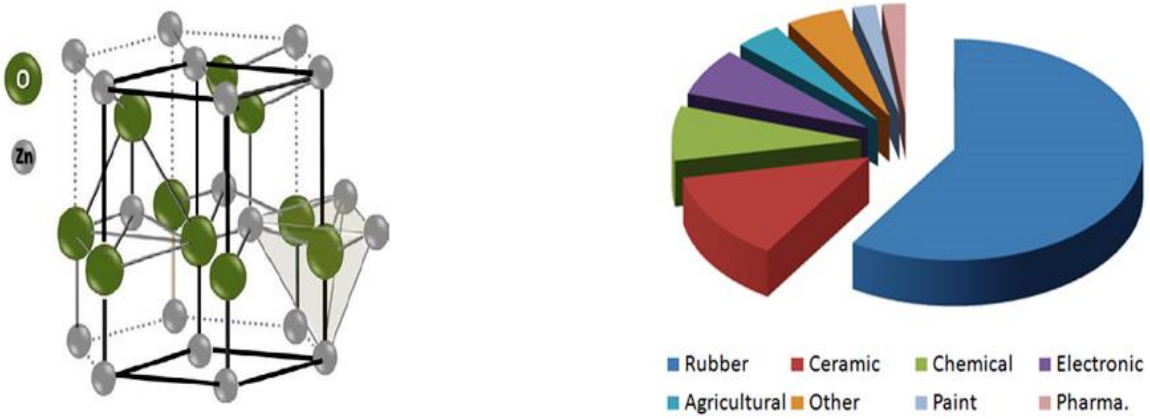

Figure 3 – The wurzite crystal structure [21] and worldwide applications of Zinc Oxide. [16]

ZnO can be produced in the chemical reaction of zinc with water at 500 °C. When it is produced through zinc in contact with air, a protective layer is formed which prevents further metal oxidation. In ceramics production it reduces the temperature and the energy for the melting. In pharmaceutical industry it is present in lotions and sun creams. The piezoelectric proprieties of ZnO are due to the wurzite crystal structure. The regular and symmetric hexagonal crystalline structure and the electric dipoles create polarization growth. [22] It has application on batteries because when an electrode is a piezoelectric material performs at high voltage. The high electrochemical coupling efficiency is the ratio of electrical energy to acoustic energy

which is 1.2 cm^{-2}. [23] When the temperature increases in the cell it is produced a voltage which corresponds to the polarization. When their temperature decreases, a voltage develops having the orientation opposite to the polarization. [24] ZnO is an n semiconductor that can be p doped easily for the use in electronics such as a gas sensor of UV radiation. [25] It has the highest excitation energy of all the semiconductors of groups II-VI and III-V. The dual behavior of working as an ionic and covalent semiconductor is explained by the electronic configuration of zinc [Ar] $3d^{10}$ $4s^2$ which the direct band gap is 3.4 eV. It has high electronic binding energy of 60 meV and electron mobility higher than 100 cm^2 $V^{-1}s^{-1}$. It is a constituent of LED´s, laser diodes [26] and solar cells. [27]

Table 2 Chemical and physical proprieties of ZnO at 25 °C. [28]

Electron Mobility (cm^2/ Vs)	> 100
Electron binding energy meV	60
Direct Bandgap eV	3.3 – 3.4
Crystalline structure	Hexagonal (wurzite)
Lattice constant (a) (nm)	0.325
Lattice constant (b) (nm)	0.521
Color crystalline form and refractive index	White, amorphous, 2.004
Specific gravity	5.606
Molecular weight (g mol^{-1})	81.34

2.1.1 ZnO composites electrodes and metal organic frameworks electrodes

In the last years, the capacity fading of ZnO during cycling has been reduced by doping this material with some chemical elements forming composites, zeolites or metal organic frameworks. Porous materials have been tested as electrodes due to the new elements when added to the zinc oxide behave themselves as catalysts that retard the degradation of the zinc oxide in the electrode and therefore, provide less capacity degradation, high reversible capacity, stability and good cycling performance than common synthesis of ZnO electrode due to the higher storage of lithium ions and shorter path for ions diffusion. [29]

A ZnO-composite made with nickel showed 466 mAh g^{-1} reversible capacity after 120 cycles confirming better battery cycling due to less volume expansion and less capacity fading

comparing with the reversible capacity of 100 mAh g^{-1} in the 12th cycle at the same current density of ZnO. [30] Cupper when added to the ZnO electrode in the ratio of 1:4 revealed a discharge capacity of 1372 mAh g^{-1} and a reversible capacity of 962 mAh g^{-1} and at the 100th cycle it shown a reversible capacity of 819 mAh g^{-1}. [31]

Recently, the composite Zn_2SnO_4 led to an irreversible capacity of 1249 mAh g^{-1} and reversible capacity in the first cycle of 873 mAh g^{-1} which corresponded to the Coulombic efficiency of 6 %. [32] A reversible capacity of 546 mAh g^{-1} in the 100th cycle was achieved. Less capacity fading than ZnO electrode was shown and electrode durability last till the end of the 50th cycle with 357 mAh g^{-1} of reversible capacity. The first irreversible capacity of $ZnSnO_2$ and ZnO was 1300 mAh g^{-1} and 690 mAh g^{-1} respectively. [10] Porous electrode Zn_2SnO_4 showed an improved cycling comparing to the respective composite. In the 20th cycle the reversible capacity of the porous electrode was 380 mAh g^{-1} of and the electrode non-porous was around 100 mAh g^{-1}. The porous electrode Zn_2SnO_4 had an irreversible capacity of 1180 mAh g^{-1} and 380 mAh g^{-1} . For the electrode non-porous the irreversible capacity in first cycle was around 1300 mAh g^{-1} while the reversible capacity was 380 mAh g^{-1}. [33]

The composite ZnO-Si revealed that the higher the amount of silicon in the composite produces a higher reversible capacity. The ZnO electrode showed a reversible capacity of around 220 mAh g^{-1} during in the 20th cycle while the ZnO-Si composite, 480 mAh g^{-1}. However, the capacity fading is lower for the ZnO electrodes, in the composite it was shown that the capacity fading is not dependent on the amount of Si because the lower the capacity fading corresponded to the medium value of Si present in the composite. [11] Another study with ZnO nanocrystals coated with Si using the chemical vapor composition showed an irreversible capacity of 3644 mAh g^{-1} and reversible capacity of 3124 mAh g^{-1} corresponding to 86 % of Coulombic efficiency but it increased in the following cycles to 99 % and kept nearly stable. In the 100th the cycle the reversible capacity was 2600 mAh g^{-1} and the Coulombic efficiency was 95 %. [12]

The performance of the ZnO-SnO_2 composite was investigated in different ratios as well as different milling time. The composite with higher ratio of SnO_2 exhibited the best cyclability and lower capacity fading with 20 h of optimum milling time comparing with the composite with equal ratios of ZnO and SnO_2 which had the same optimum milling time. This reveals that SnO_2 improves significantly the electrode performance. Non-milled ZnO has shown the values of irreversible capacity and reversible capacity of 1194 mAh g^{-1} and 359 mAh g^{-1} respectively while ZnO-SnO_2 milled for 20 h revealed 1484 mAh g^{-1} and 667 mAh g^{-1}.[34]

A comparison between the performance of cobalt and iron in the composites with ZnO was made knowing that Co has lower weight than Fe. It was revealed that $Zn_{0.9}Fe_{0.1}O$ had reversible capacity of around 750 mAh g^{-1} in the 10th cycle while the ZnO had the reversible capacity of around 380 mAh g^{-1} in the same cycle. In the same ratio, the composite $Zn_{0.9}Co_{0.1}O$ showed a

reversible capacity of around 970 mAh g^{-1} and revealed capacity stability of 920 mAh g^{-1} from the first cycle till the 30th cycle.[35]

The addition of alumina to the ZnO electrode showed discharge capacities of 1513 mAh g^{-1} and 490 mAh g^{-1} for the 1st and 100th discharge, respectively. The capacity of the ZnO electrodes at the 1st cycle was 415 mAh g^{-1}. The composite increased 20 % of the capacity retention comparing with the ZnO electrode.[36]

Gold when added to zinc oxide revealed an irreversible capacity of 1280 mAh.g^{-1} comparing with the ZnO electrode (925 mAh g^{-1}). At the 50th cycle the reversible capacity is constant for the ZnO-Au hybrid electrode while the reversible capacity is 225 mAh g^{-1} for the common ZnO electrode.[37]

Vanadium, when added to the electrode ZnO, delivered a reversible capacity of 575 mAh g^{1} after 200 cycles, revealing high stability and good reversible capacity. [38]

Recently ZnO zeolite was utilized as electrode in lithium-ion battery showing irreversible and reversible capacity of 954 mAh g^{-1} and lower capacity fading in the 20th cycle. [39] Zeolite ZnO/$ZnFe_2O_4$/C has revealed to have 1500 mAh g^{-1} of reversible capacity in the first cycle and 1050 mAh g^{-1} in the 100 cycle. [40] Zeolite cobalt in a ZnO framework has shown a reversible capacity of 725 mAh g^{-1} at the 50th cycle while the ZnO while ZnO has reached 355 mAh g^{-1} in the same cycle at the same current density.[41]

Porous hybrid ZnO with cupper showed a reversible capacity of 818 mAh g^{-1} after 100 cycles with 100 % capacity retention. The first irreversible capacity was 1372 mAh g^{-1} and the reversible capacity was 962 mAh g^{-1} which proves stable capacity during cycling.[31]

Porous electrodes promise even better electrodes than composites electrodes. They have high conductivity, cycling performance and less volume expansion during lithiation and delithiation. This is due to the free interstitial space which allows lower electrode stress and therefore keeps the electrochemical performance of the electrode. Their large interfacial area and double-layer adsorption enables the reactants to stay near the electrode surface and therefore provides sustained values of reversible capacity during cycling, lower ohmic losses, better diffusion of ions and permits separation from potential contaminants.[33]

The electrochemical proprieties of ZnO this material reveals the potential for new and more chemical synthesis methods of zinc oxide. Some other important criteria in the development of new components for lithium cells are low cost of raw materials, easy synthesis and non-toxicity. The data obtained in the performance of the batteries depends on the mechanical and chemical methods of the electrodes synthesis; C rates chosen and other variables which must be known in other to compare electrode materials. Moreover the production of ZnO composites electrodes and zeolites is more expensive than the ZnO electrode and one parameter in selecting a

material for electrode in high capacity batteries is low cost materials. Thus, it is important to investigate the best methods to utilize in synthesis and electrode fabrication.

2.2 Synthesis of zinc oxide and its influence in the cycling performance

2.2.1 Synthesis of zinc oxide

Zinc oxide can be synthetized through mechanical processes and chemical processes accordingly to a wide range of applications. Mechano-chemical processes include ball milling, controlled precipitation, precipitation in the presence of surfactants, sol-gel process, solvothermal hydrothermal and microwave techniques, solvothermal, hydrothermal and microwave techniques. Chemical processes are the emulsion and micro-emulsion environment. (Annex 1)

ZnO micro rod arrays were synthetized through the chemical bath deposition. The reactant 0.04 mol zinc acetate dihydrate, 0.5 mL ethylenediamine, and 150 mL distilled water. After being dried at 65 °C the solution was deposited during 1h on a cupper foil a copper foil, ultrasonic cleaned with acetone and ethanol that suspended horizontally in the solution. It was washed with ethanol and then dried inside a quartz tube furnace in flowing argon at 350 °C for 30 min. [42] ZnO particles were also produced by the thermal process in order to understand the differences of electrodes with the conductor graphite. For the electrode with graphite, a dispersion made of 30 mg of graphite, 60 mL of water was left in sonification for 3 h. After this 3 mol of $Zn(NO_3)_2.6H_2O$ and NH_3 with water in 25 of wt. % was added to the dispersion for pH of 8. The dispersion was transferred to a Teflon-lined stainless steel autoclave (100 mL) and heated for 8 h in an electric oven at 150 °C. [43]

Zinc oxide was synthetized by solution phase. KOH (4M) and $Zn(NO_3)_2.6H_2O$ (0.5 M) were prepared in separated bottles by dissolution in water and then mixed together and the final solution was contained in a 50 mL Teflon autoclave during 12 h at room temperature. The substrate was disposed in a zinc sheet, washed with water and ethanol and dried during many hours at 85 °C. [37]

Utilizing the disposition method of microwave assistance, $(CH_3COO)_2Zn{\cdot}2H_2O$ (1.5 M) was mixing together at 720 w with KOH (0.5 M) to have pH equal to 8. It was found out that the reaction took place at 80 °C after 30 min. The mixing solution was disposed in intervals of 2 s and rest in intervals of 3 s. Afterwards the product ZnO formed a colloidal suspension with ethylene glycol. Graphite nanosheets were added to the suspension at room temperature in a high-performance homogenizer during 30 min following by drying inside a vacuum oven for 12 h at

105 °C. The nanosheets were then dried inside an oven at 400 °C in a ratio of H_2:Ar of 5:95 in v/v. Three types of nanosheets were produced differing in amount of graphite. [44]

ZnO was synthetized through the solvothermal method with porous carbon and without porous carbon. $Zn(CH_3COO)_2 \cdot 2H_2O$ (2 g) was mixed with 14 mL polyethylene glycol and 76 mL of ethanol solution. Porous carbon was synthesized with gelatin and $CaCo_3$ in the ratio 2:1 and calcinated in argon atmosphere at 700 °C during 2 h and added to the previous solution in different amounts. The mixture was transferred to a 100 mL Teflon-lined autoclave and mixed with 0.7 g of solid NaOH, sealed during 24 h at 140 °C and cooled down at room temperature. The resulting precipitated was filtered off, washed and dried during 10 h at 50 °C. [45]

ZnO with alkaline solution was produced *in situ* through co-precipitation process. Polyvinylpyrrolidone (0.5 M) was added to 100 mL of deionized water at 60 °C. Carbon nanotubes were dispersed in dimethylformamide solution (2 M) after 20 min $ZnCl_2$ was added to the above solution and sonicated at room temperature. The pH was adjusted to 11 with ammonia (5 M) under ultrasonic agitation during 2 h. The precipitates were washed, dried and heated during 1h at 500 °C. [46] The zinc oxide synthetized with zinc(II) gluconate hydrate and deionized water led to the ion concentration of 0.2 M. The solution was mixed with sucrose (1.2 M) and stirred at room temperature for 15 min, the sucrose decomposed and the water was evaporated. The slurry was dried and calcinated during 3 h. [35]

In this work, zinc oxide was synthetized through ball milling because this mechanical method was found to enable the best particle reduction and therefore large surface area of the active material. [47]

2.2.1.1 Mechanical Milling

The mechanical milling is a process in which the reactants are mixed with small metal balls that create a high particle impact through speed rotation of a milling machine. These conditions allow large surface of active material to an optimum value of milling time which corresponds to the lowest size of particle reduction. There are different types of milling machines such as vibrational mill, planetary ball mill, mixer mills and stirred ball mills. The reactants mixing can be operated at dry where it depends on the vacuum pressure and gas atmosphere or at wet in which the liquid mixing depends on the physical proprieties such as density, chemical stability and parallel reactions. Their conditions are dependent on the powder to ball ration, the milling atmosphere which can possible contaminate the mixture, milling time and milling speed.

There are three different stages of milling. The first corresponds to the Rittinger stage in which almost of the energy input leads to the surface area production. The following stage is the aggregation stage where there is particle aggregation and therefore the energy available to

reduce particle size is lower than the input energy. The third stage is the agglomeration stage in which there is a growth in dispersion following by drop and stop of agglomeration. At this stage the surface area is reduced due to the agglomerates. This is dependent chemical and physical proprieties of the host material, usually carbon black and the binder.

The temperature affects the milling. For the same milling time, the higher speed rotation, the number of metal balls and their size the higher is the temperature [47]. Experiments revealed that at higher temperature ZnO is more conductive. [48]

For the synthesis of ZnO through ball milling, ZnO commercially size of 500 nm with purity of 100 % was mixed within a steel cylinder in a ball to power ratio of 1:14 with a horizontal oscillatory mill (Retsch MM2). [49] Damonte et al [34] came to the conclusion that particles had the grain size of 20 nm and the surface area increased with 5 h of ball milling.

2.2.2 ZnO electrode fabrication

The method to fabricate the electrode must be one that originates a thin electrode thickness in order to facilitate the electron diffusion across the electrode to its surface where the redox reactions take place. This is possible monitoring the best parameters in the fabrication methods, such as tape casting (doctor blade method), thermal vapor decomposition, and spray coating method.

ZnO synthetized through ball milling (11.6 %) and then mixed together with upper S carbon (1.4 %), polyvinylidene fluoride (PVDF) (5.5 %), propylene carbonate (9.5 %) and acetone (72 %). The slurry was stirred at 50°C during 4 h, dried on glass and the propylene carbonate was separated. This electrode resulted in an irreversible capacity of 1000 mAh g^{-1} and reversible capacity of 412 mAh g^{-1}. The electrode ZnO which was not milled resulted in an irreversible capacity of 1194 mAh g^{-1} and reversible capacity of 359 mAh g^{-1}. [34]

The electrode from ZnO micro rod array synthetized through chemical bath deposition [42] was fabricated with slurry coating and without binder. The procedure consisted in mixing the microrods with acetylene black, the N-methyl pyrrolidinone (NMP) solution of PVDF. The slurry was then spread the on the copper foil substrate. The microrod powder electrode was made with mass ratio of ZnO, acetylene black and PVDF of 80:12:8 by normal slurry coating. In the microrod electrode, with 78.5 % and Coulombic efficiency and a reversible capacity over 600 mAh g^{-1}. The capacity fading was much less for the electrode microrod array and it had higher first discharge almost 800 mAh g^{-1} while the microrod powder electrode was 700 mAh g^{-1}.

The electrodes produced by the thermal process were made mixing with a magnetic stirring PVDF, acetylene black and NMP in the ratio 75:15:10. The mixture was disposed on nickel foam and dried at 100 °C in vacuum for many hours. The electrode with graphite showed an

irreversible discharge of 1235 mAh g^{-1} and a reversible discharge of 420 mAh g^{-1}. For the electrode without graphite, the capacity dropped faster and reached the value of 100 mAh g^{-1} at the 25th cycle while the electrode with graphite has 325 mAh g^{-1} of reversible capacity in the same cycle. [43]

Zinc oxide electrode prepared by the solution phase lead to the irreversible capacity of 958 mAh g^{-1}, reversible capacity of 590 mAh g^{-1} and a Coulombic efficiency of 52 %. The reversible capacity is stable at 200 mAh g^{-1} from the 10th cycle to the 50th cycle.[37]

The electrode ZnO with different graphite ratios was produced with the PVDF binder and the conductors Super-P and KS-6 in the respective ratios of 82:10:4:4. The slurry was prepared with NMP solvent, mixed during 3 h with Zr balls and pasted on a cupper foil through the doctor blade method. The solvent was evaporated with a blow dryer. Inside a vacuum oven the sheets were dried during 12 h and under 200 $kg.cm^{-2}$ of pressure. The electrode had the final thickness of 100 μm. It was found out that the electrode without graphite Coulombic efficiency of 49 % and irreversible capacity of 606 mAh g^{-1}. The electrode with higher graphite ratio showed a reversible capacity of 850 mAh g^{-1}, higher Coulombic efficiency of 82 % and lower capacity decay (8 %). After 50 cycles the reversible capacity is higher for the electrode with more graphite (460 mAh g^{-1}), in which the ratio of ZnO is equal to the ratio of graphite. [44]

The electrochemical test was made with electrodes ZnO by coating the slurry of active material, carbon black and PVDF in the ratio of 6:2:2 dissolved in methyl pyrrolidinone. The resulting mixture was dried on a cupper foil during 10 h at 100 °C. The electrode ZnO with porous carbon prepared by the solvothermal method revealed with the highest ratio of carbon black (2:1) revealed the value of discharge capacity of 654 mAh g^{-1} after 100 cycles. The electrode without carbon black showed a reversible capacity of 123 mAh g^{-1}. The first discharge capacity of the ZnO electrode with the highest amount of carbon was 2050 mAh g^{-1} while the electrode without carbon black was 1250 mAh g^{-1}. [45]

The electrode zinc oxide with carbon in the ratio of 4:1 revealed first discharge capacity of 820 mAh g^{-1} and reversible capacity of 220 mAh g^{-1}after 100 cycles. [17]

The electrode ZnO synthetized with carbon nanotubes and PVDF was prepared in the ratio 8:1:1 respectively, dissolved in NMP solvent and disposed in a nickel foil. The coated slurry was left in drying for 24 h inside a vacuum oven at the temperature of 120 °C. The resulting first discharge for the electrode without carbon was 1400 mAh g^{-1} and for the electrode with carbon was 1600 $mAh.g^{-1}$. In the 50th cycle the reversible capacity of the first electrode was 450 mAh g^{-1} while the second electrode was 220 mAh g^{-1}. [46]

The electrode ZnO synthetized through ball milling was prepared with 75 % of ZnO, 20 % of carbon and 5 % of sodium carboxymethyl cellulose (CMC) (1.25 wt. %) was added to the mixture

and ball milled during 2 h. The slurry was disposed in dendritic copper foil and doctor blade method was utilized for casting and then it was dried inside a vacuum oven during 12 h at 120 °C. This electrode revealed a first discharge capacity of almost 700 mAh g^{-1} and at the 10^{th} cycle the reversible capacity is 380 mAh g^{-1}.[35]

2.2.2.1 Tape Casting (Doctor Blade)

The electrode fabrication method tape casting consists in casting the liquid mixture on a ceramic surface to form a thick film. This liquid mixture contains among other components a binder that confers integrity and adhesion to the substrate. A speed is chosen as well as the thickness to apply to the coating of this mixture.

The mixture is deposited within a metal container with the desired thickness, on the surface of a flat metal foil, usually cupper which lies on the ceramic surface of the doctor blade machine. The machine pushes this mixer container at a constant speed which enables an homogeneous coating on the surface of the foil. The electrode fabrication tape casting is performed under vacuum and it dependence on the viscosity and tensile forces of the mixture. The objective is to produce a coating with a cohesive and homogeneous surface during drying, high mechanical strength, pyrolysis and thermocompression.

2.2.3 Electrochemical reactions between ZnO anode and Li cathode

When current is applied to the cell, simultaneously, the following redox reactions occur in each electrode:

Oxidation reaction in the anode: $ZnO\ (s) \rightarrow Zn^{2+}\ (s) + O^{2-} + 2\ e^-$

Reduction reaction in the cathode: $Li^+\ (s) + 1\ e^- \rightarrow Li\ (s)$

The respective cell representation is:

$$ZnO(s)|Zn^{2+}(s)||Li^+(s)|Li(s)$$

In the first cycle the first discharge consists of two irreversible steps: the first step corresponds to the formation of lithium oxide and the highest amount of capacity (see figure 5).

The step 1 corresponds to the reduction of zinc oxide to metal zinc and formation of amorphous lithium oxide. The following step consists in the reaction of metal zinc with lithium ions and formation of the lithium-zinc alloy (step 2).

$$ZnO\ (s) + 2\ Li^{+}\ (s) + 2\ e^{-} \rightarrow Zn\ (s) + Li_2O\ (s) \quad (step\ 1,\ 659\ mAh\ g^{-1})$$

$$Zn\ (s) + Li^{+} + 1\ e^{-} \rightarrow LiZn\ (s) \quad (step\ 2,\ 328\ mAh\ g^{-1})$$

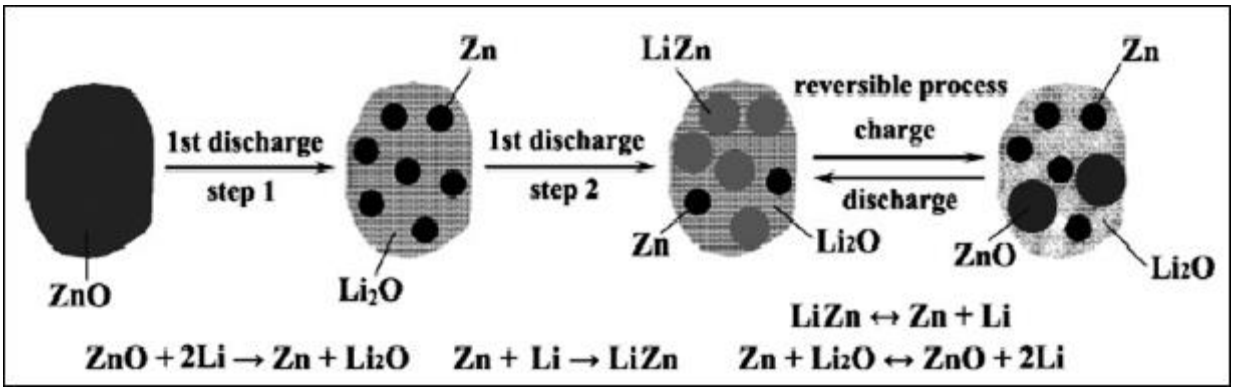

Figure 4- Electrochemical process between the electrodes ZnO and Li during the discharge and charge of the battery [50]

During discharge lithium ions shuttle into the layers of the zinc oxide while in the charge, in ideal state, these lithium ions are released back to the cathode and there is formation of metal zinc and zinc oxide (reversible reactions).

In the following cycles, lithium alloys Li_xZn are formed accordingly to the number of lithium ions x:

$$ZnO\ (s) + 2\ Li^{+}\ (s) + 2\ e^{-} \leftrightarrow Zn\ (s) + Li_2O\ (s) \quad (step\ 1)$$

$$Zn\ (s) + Li^{+} + 1\ e^{-} \leftrightarrow LiZn\ (s) \quad (step\ 2)$$

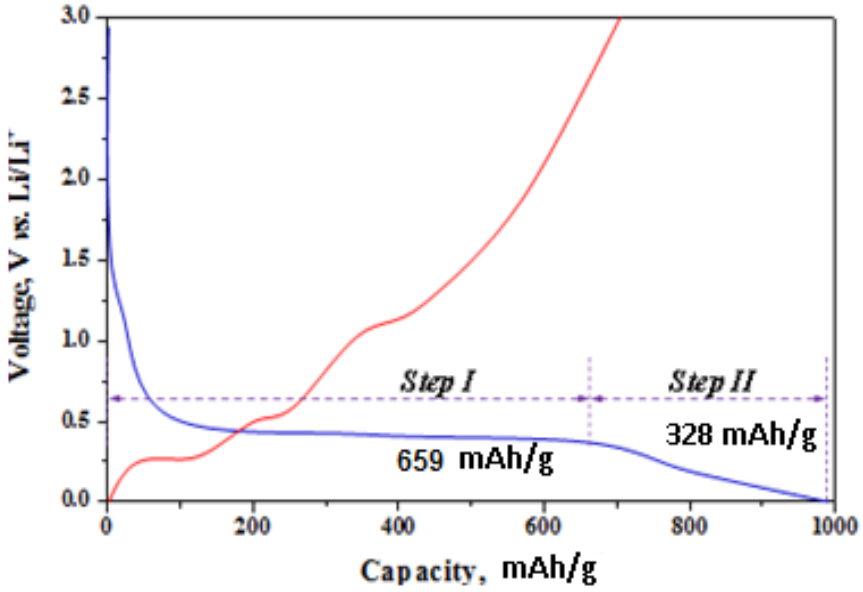

Figure 6 – Discharge and charge capacity profiles of ZnO in the first cycle

The volume expansion predicted is low due to molecular volumes of ZnO, Zn and Li_2O which are 14.5 cm^3 mol^{-1} , 15.2 cm^3 mol^{-1} and 14.8 cm^3 mol^{-1}.

3 Experimental work

3.1 Synthesis and preparation of active materials

The first part in the experimental work corresponded to the ZnO electrode prepared with ZnO commercial powder. It was followed by the synthesis of ZnO powder and afterwards the respective electrode fabrication. The third type of electrode was made of ZnO commercial suspension. For the ZnO powder synthesis, $ZnCl_2$ (Aldrich) was mixed with $H_2C_2O_4.H_2O$ (Merck) in the ratio 1:2. The mixing was carried out in a Planetary Ball Mill (Retsch PM 400 MA_type) at 300 rpm for all samples at times of 1 h, 2 h and 3 h of ball milling. A stainless steel vessel with 27 stainless steel balls with 10 mm of diameter was used. After the milling, the ZnC_2O_4 was separated from the balls carefully due to the release of HCl gas:

$$ZnCl_2\ (s) + H_2C_2O_4.H_2O\ (aq.) \rightarrow ZnC_2O_4.H_2O\ (aq) + 2\ HCl\ (g)$$

Afterwards this compound was calcinated inside a vacuum oven from 25°C to 450°C for and from 450°C to 25°C taking 6h in average. The reaction is described as follows:

$$ZnC_2O_4.H_2O\ (aq) \rightarrow ZnO\ (s) + 2\ CO_2\ (g) + 2\ H_2O\ (g)$$

Zinc oxide synthetized powder milled for 1 h, 2 h and 3 h of ball milling was named as ZnOs1, ZnOs2 and ZnOs3 samples, respectively. For the electrode preparation, zinc oxide synthetized was added with the binder carboxylmethyl cellulose 5 wt % (Na-CMC, Merck) and sodium salt Na_2Co_3 (Merck) and the conductor component CB 99 % (carbon black Super P, Afa Aesar) in the ratio of 4:0.5:0.5 with 5 mL of water to improve the solution homogeneity was added to stainless steel vessel. Each one of the three samples (ZnOs1, ZnOs2, ZnOs3) were milled for 3 h and zinc oxide was produced.

For comparison, the same ratio of ZnO:CMC: carbon back was used for all electrodes. First the powder was milled for 1 h with carbon black and then this mixture was added the CMC dissolved in water in different amounts. This was carried out to test the viscosity and the water influence in the doctor blading coating. The obtained ZnO electrode commercial corresponds to ZnOc4. Finally, ZnO electrode with 50 wt% ZnO suspension (Aldrich) was fabricated (ZnOsp) through ball milling of 3h.

The mechanical milling was performed in a ball milling machine Retzsch PM 400. Several different slurries were inserted with different milling times for mechanical alloying of the

electrode and homogeneous mixture with the optimum particle size. The speed rotation applied was 300 rpm for all samples.

3.2 Fabrication of zinc oxide electrodes and cells

The method utilized in the fabrication of zinc oxide electrode was tape tasting. The machine utilized was MSK–AFAI Automatic Thick Film Coater. The electrode slurry was deposited on a cupper foil with 100 µm wet-thickness for the electrode. At the end was obtained the cupper foils of: ZnOs1, ZnOs2, ZnOs3, ZnOc4, ZnOsp. Each one was disposed inside a vacuum oven (HERAEUS) for around 12 h.

Table 3 bellow presents the milling times of the ZnO and CB, CMC and H_2O and the corresponding thickness of the electrodes. The milling time of the powder and the milling time of the CB, CMC and H_2O as well as the electrode thickness of the ZnO electrodes are shown in the table 4.

Table 3 - Mechanical milling parameters and dry thickness obtained from the tape casting for the zinc oxide electrode commercial and zinc oxide suspension.

	Mechanical Milling	Tape Casting (Doctor Blade)
Sample	**Milling time ZnO & CB (h) + CMC & H_2O (h)**	**Dry thickness (µm)**
ZnOc4	1+2	42
ZnOsp	3	42
$ZnOs_1$	1+3	42
$ZnOs_2$	2+3	40
$ZnOs_3$	3+3	40

The samples corresponding to each electrode were labeled with numbers for many parameters in the electrochemical tests. Each electrode was weighted, dried again and measured its corresponding thickness. Before assembling the electrodes were pressed at 20 kg cm^{-2}. (Annex 3) Then they were disposed inside a glove box which works in vacuum and it does not allow contaminations.

Figure 7 - Glovebox utilized in the construction of the half-cells.

The Swagelok half-cell (Figure 7) consists of several steel pieces which are screwed, closed and hold inside the electrodes ZnO and Li and the electrolyte. The electrolyte was $LiPF_6$ (1 M, EC:DMC of 1:1, v/v) and it was added 20 µL of solution between the electrodes. The anode collector was made of stainless steel. The separator utilized between the electrodes was Polypropylene (Celgrad 2400®) with the thickness of 40 µm. Both electrodes and separator were cut in circles with the diameter of 1 cm.

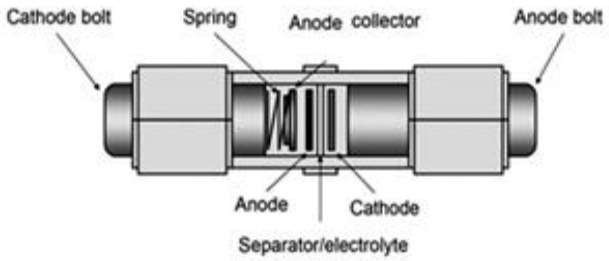

Figure 8- Representation of the Swagelok half-cell

3.3 Electrochemical characterization

The electrochemical tests applied were the cycling at 0.05 C rate and 0.2 C rate. It was analyzed the ZnOc and ZnOsp (micro-size and nano size), the influence of milling time of ZnOs electrodes, the Influence of pressing the electrodes, the comparison of unpressed and pressed electrodes. The cycling was performed with minimum voltage 0 V and maximum of 4 V, with the range between discharge and charge 0.02 V and 3 V respectively. The Basytec® software was utilized in the electrochemical characterization of the different electrodes. Every half-cell

was connected to an external circuit which was connected to the computer and allowed the collecting of all respective data.

Figure 9 - Montage of the half-cells in the electrochemical testing

3.4 Structural and chemical characterization

The electrodes surfaces were analyzed using XRD and SEM techniques in order to relate the cycling performance and milling time with the amount of active material disposed, its particle size and shape. The XRD diffractograms were performed with an X-ray diffractometer D8 Discover GADDS, which detector area was was VÅNTEC-2000. The accelerating voltage was 45 kV and the tube current was 0.650 mA. A tuned monochromatic and parallel X-ray beam (Cu-Ka) with a tube collimator aperture of 1 mm was utilized for each exposures which last 180 s.

The SEM analysis was obtained with Zeiss ULTRA plus with Charge Compensation with the accelerating voltage was 1 kV and the secondary electron detector was used for the observation of the morphological changes on the zinc oxide surface.

4 Results and Discussion

4.1 Morphology of electrodes

The surface and morphology analysis obtained through SEM underline the difference between the commercial and the synthetized active material (see Figure 10). The active materal ZnOc commercial had the biggest particles in the form of hexagonal crystals corresponding to the micro-size. The active material ZnOsp suspension had the particles in the lowest size, corresponding to the nano-size.

The synthetized active material, ZnOs1 revealed plank structure in their particles which corresponds to the beginning of pulverization and it is due to the lowest milling time set in the mechanical milling. As the milling time increased for the ZnO synthetized, the active material ZnOs2 had the mixed structure of nano-particles and plank particles while ZnOs3 had the highest milling time and nano-plank particles resulting from the aggregation of the nano-particles. (Figure 10)

There is a relation with the milling time and the particle size of the active materials. As the milling time increases the plank structure of ZnO pulverizes and forms tiny aggregates due to the forces applaied on the active material inside the vessel of the mechanical milling machine. For higher milling times applaied the tiny particles agglomerate and form big aggregates because the electrostatic forces and *van der wall* forces that allow their attraction and cohesion. Accordingly to the electric field concept, these particles have different charges (positive and negative) that results in their attraction. The *van der wall* forces are the dipole-dipole intermolecular interactions between the zinc cations and oxygen anions.

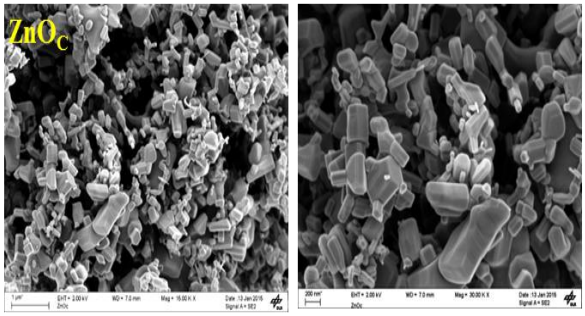

Hexagonal structure; particle dia. = 40 ~ 300 nm

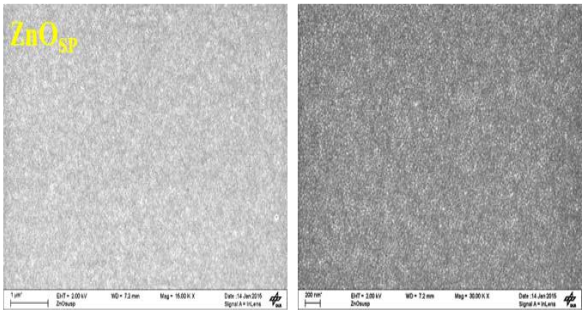

Hexagonal structure; particle dia. = ca. 35 nm

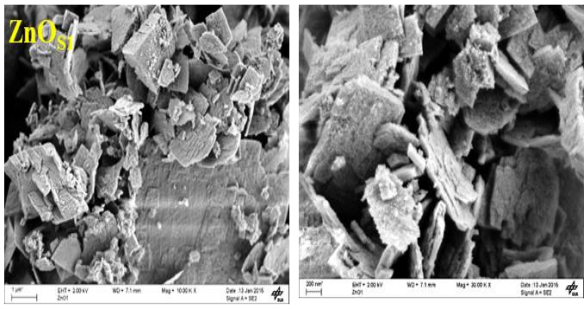

Plank shape

Mixed structure

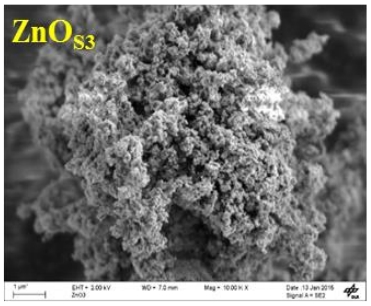

Aggregated nanoplank

Figure 10 – Morphology and surface pictures obtained in SEM analysis before cycling of ZnOc, ZnOsp, ZnOs1, ZnOs2 and ZnOs3.

4.2 XRD

The analysis XRD of the electrodes slurry before cycling showed broadening of peaks due to the reduction of particle size from micro-size to nano-size obtained with the mechanical milling of the ZnOc and ZnOsp respectively (Figure 11).

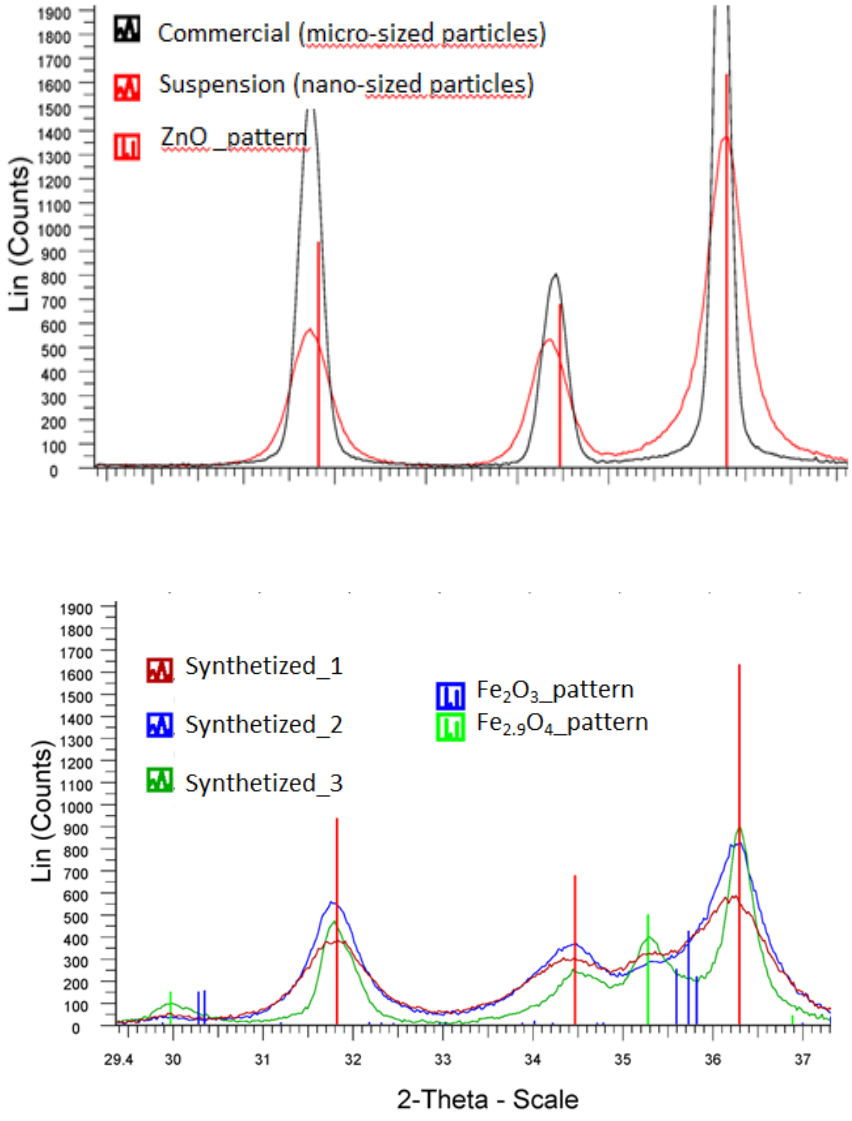

Figura 11 – Crystal structure analysis of the ZnOc, ZnOs and ZnOsp obtained through XRD before cycling.

The observation of the peaks revealed the existence of contamination with Fe_xO_y with increasing of milling time. Therefore ZnOs1 has the lowest contamination of all the synthetized electrodes due to the the lowest milling time. The forces and speed rotation of the stainless

steel balls into the same material vessel in which the active material was millied contained the electrode slurry induced contamination in the ZnO electrodes.

The oxidation of the stainless steel materials was also induced by the chloridric acid and water released during the formation of the intermediary components and the final product, the active material. The galvanized protective layer was destroyed and the contact with iron affected the active material purity.

4.3 Comparision of ZnOc and ZnOsp (micro-size and nano size)

The half-cell with the ZnOsp showed higher irreversible capacity (near 800 mAh g^{-1}) than the ZnOc due to the particle size being nano-size which allow higher contact area with Li ions and higher conductivity. The electrode ZnOc revealed fast capacity fading in the first cycles (Figure 10).

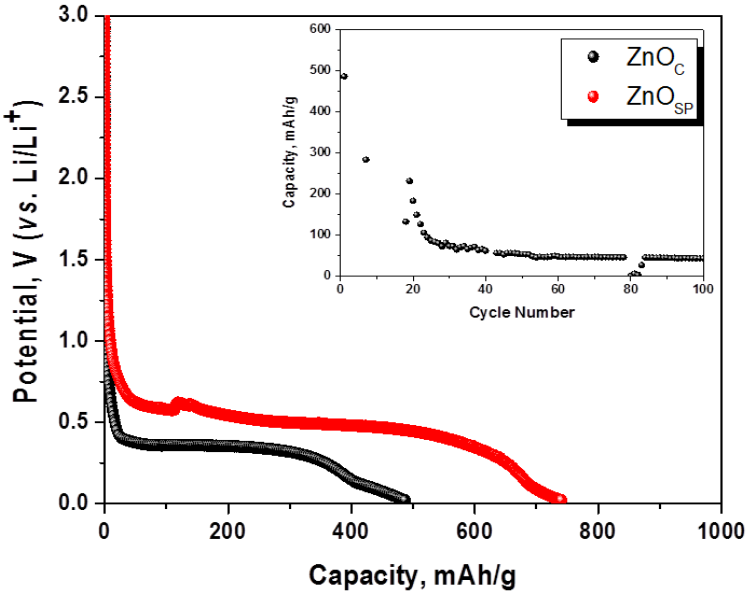

Figure 12 - Discharge capacity and cycling of the ZnOc and ZnOsp at 0.2 C rate.

Although the higher irreversible capacity of nano-size particles, ZnOsp had very small size particles which lead to increase of contact resistance and aggregation of particles during cycling resulting in capacity fading to zero after the first cycle.

The capacity fading fast during cycling was confirmed through the SEM pictures for both electrodes (Figure 13). The electrode ZnOc had micro-size particles, in the form of hexagonal crystal structure. The electrode ZnOsp had nano-size particles before cycling. The biggest size

of particles and the smallest size corresponded to electrodes resulted in insignificant cyclability for the demand of high capacity batteries.

The surface and morphology pictures of the electrodes obtained in SEM before cycling confirm the electrode performance. After cyclng it is evident the instance of the active material and the formation of cracks on the surface (yellow circles in figure 13).

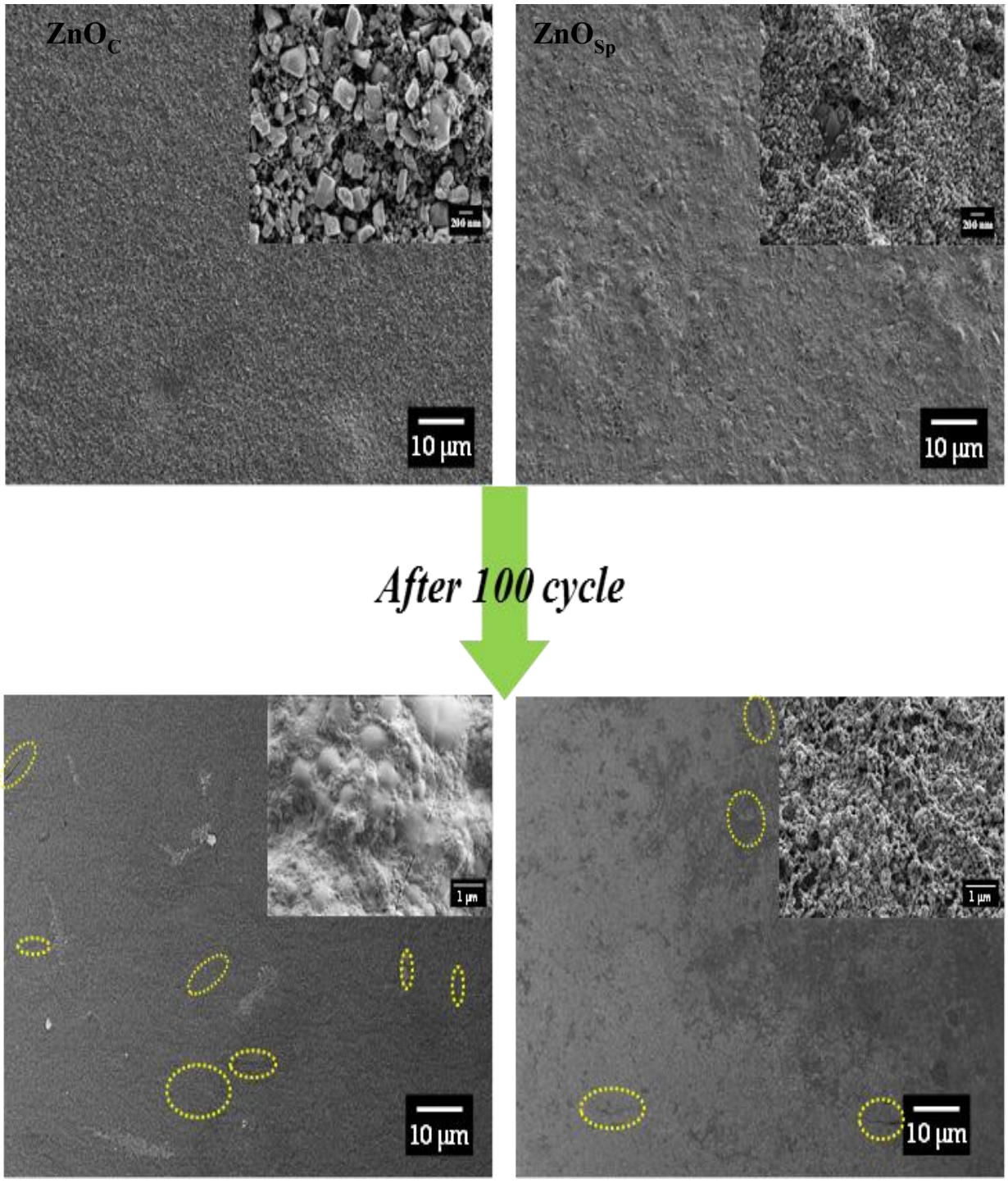

Figure 13 - SEM pictures of ZnOc and ZnOsp before and after cycling

Both electrodes revealed cracks at their surface due to the incomplete dealloying where the lithium-ions are not shuttled back to the cathode which are reflected the activation overpotential with resistance of the electron transfer across the circuit and lithium ions in the diffusional path.

4.4 Influence of milling time in ZnO_s electrodes

The half-cells with ZnO_{s1} and ZnO_{S2} reveal irreversible capacity near to 987 mAh g^{-1} corresponding to the lower milling times performed in the electrode slurry fabrication as it is shown in the graphics bellow.

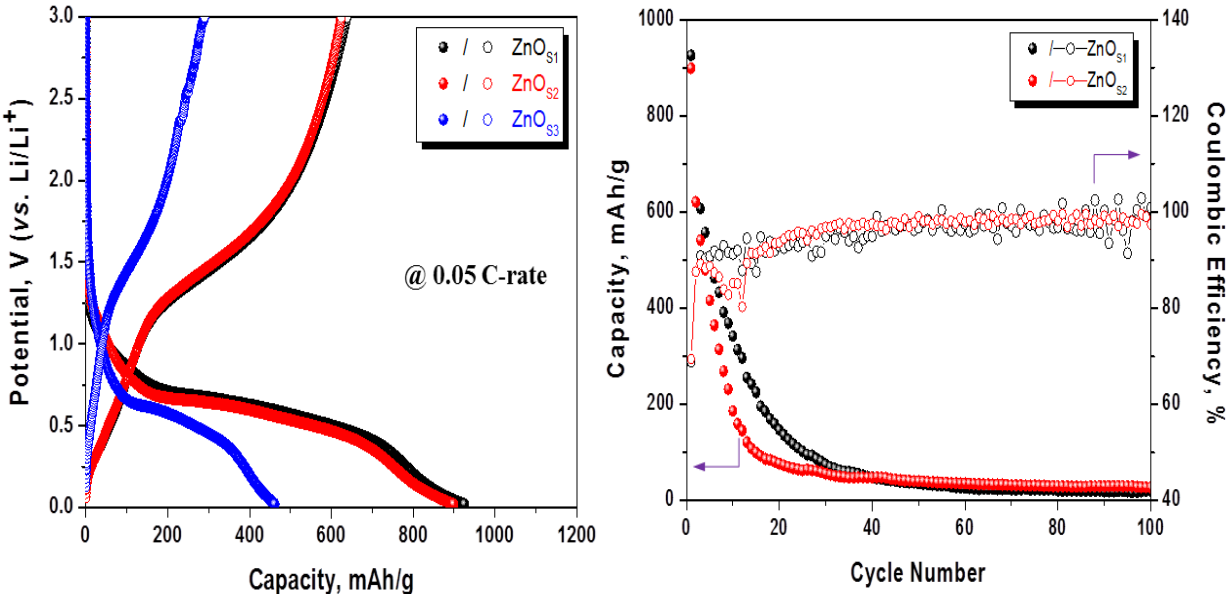

Figure 14 - First discharge capacity and cycling of the electrodes ZnOs at 0.05 C rate

During cycling ZnOs2 revealed faster capacity fading and more unstable Coulombic efficiencies than the ZnOs1. After the 20th cycle the reversible capacity is under 100 mAh g^{-1} for ZnOs2 while for ZnOs1 is 150 mAh g^{-1}. $ZnOs_3$ fade during cycling probably due to contamination with Fe_xO_y and The conditions set for the electrodes ZnO syntetized and ZnOsp were set after fabrication of the electrodes with ZnO commercial (Annex 2).

The graphics reveal that the fastest capacities fading correspond to the higher milling times. Delamination and breakdown of electrodes were observed with the SEM pictures.

4.5 Influence of pressing the electrodes

The electrodes that were pressed at 20 kg cm^{-2} revealed higher discharge capacities. Pressing increased the capacity and stability of all electrodes. (Figure 15)

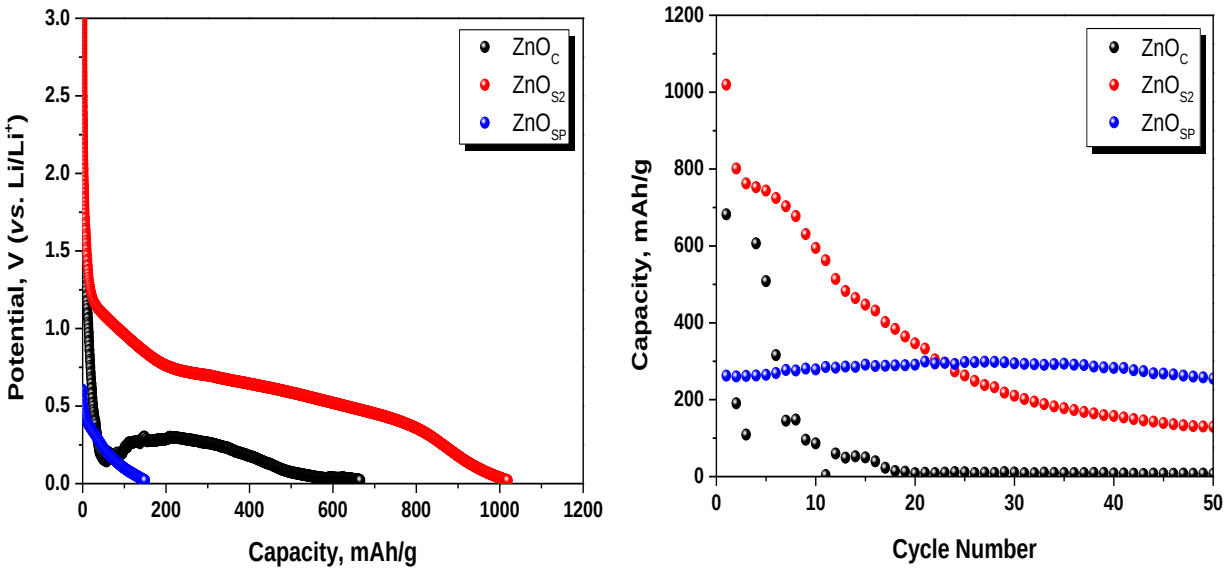

Figure 15- First discharge capacity and cycling of the electrodes ZnOc, $ZnOs_2$ and ZnOsp at 0.05 C rate (ZnOs1 revealed zero capacity since the first cycle).

The highest irreversible capacity was obtained with the electrode $ZnOs_2$ which was expected due to the lower milling time and smaller particle size that allows higher conductivity and capacity. The value of discharge capacity of ZnO_{s2} higher than the theorical (987 mAh g^{-1}) indicated the presence of impurities with iron oxides.

During cycling the capacity faded faster for the electrode ZnOc which reached the the reversible capacity zero at the 20th cycle while the electrode ZnO_{s2} reached around 300 mAh g^{-1} in the same cycle. ZnOsp showed high stability during cycling although the reversible capacity was around 250 mAh g^{-1} and the Couloumbic efficiency varies in a wide range during cycling. (Figure 16)

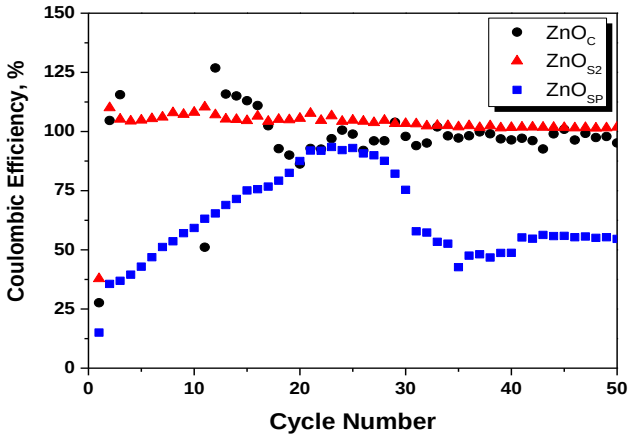

Figure 16 - Coulombic efficiency of ZnO_c, ZnO_{s2} and ZnO_{sp}

4.6 Comparison of unpressed and pressed electrodes

At the same C rate, ZnOc and ZnOs2 unpressed electrodes revealed not only lower irreversible capacities but also faster capacities fading in the first cycles at 0.05 C rate. (Figure 7)

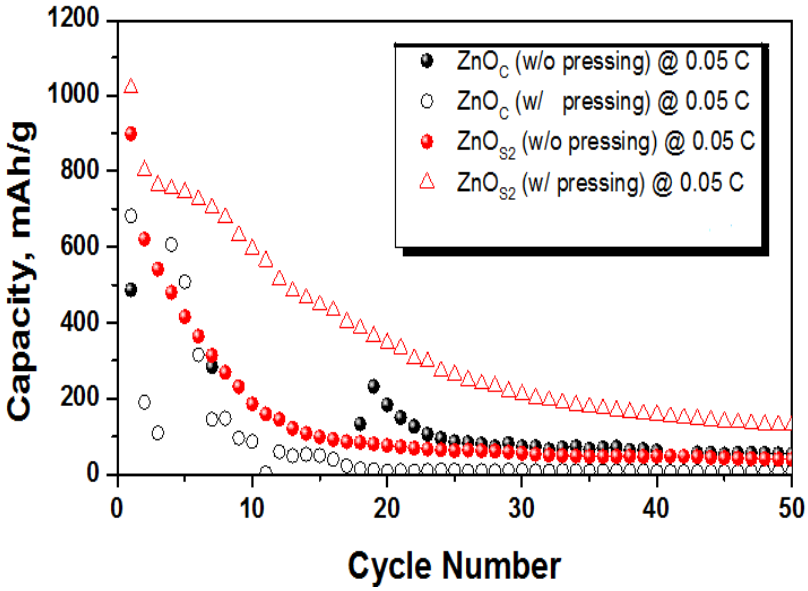

Figure 17 - Cycling of ZnOc and $ZnOs_3$ unpressed and pressed electrodes at 0.05 C rate.

As shown before, ZnOs2 had particle size in nano size revealed higher discharge capacity for both pressed and unpressed electrodes comparing with the electrode ZnOc. At the 20th ZnOs2 had the reversible capacity near 300 mAh g^{-1}.

Pressing affected the contact between the electrode and the active material through enhancement of the electrode density. In the same volume, the contact with the active material was higher which lead to the increase of conductivity and higher capacity. The effect of pressing combined with a suitable milling time that produces nano-size particles lead to higher irreversible capacities than the theorical value of 987 mAh g^{-1} due to modification of surface and morphology.

4.7 Electrochemical test of the $ZnOs_1$ pressed

The electrode with the lower milling time revealed the highest reversible capacities during cycling at 0.2 C rate of all the half-cells tested. It was shown an irrervisible capacity of 1080 mAh g^{-1} and slow reversible capacity fading during cycling (Figure 18).

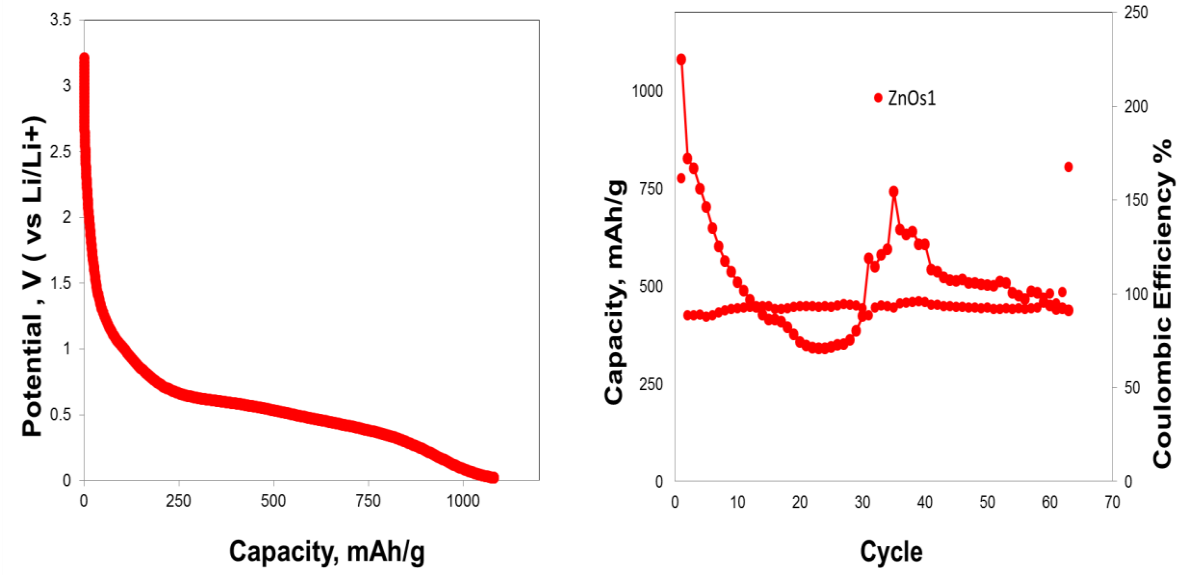

Figure 18 – Discharge and cycling testing of the electrode $ZnOs_1$ at 0.2 C rate

The electrodes ZnOc, ZnOsp and $ZnOs_2$ failed when applying the electrochemical test of discharge and cycling at 0.2 C rate. This is possible to the highest surface area increased side reactions and electrolyte decomposition and the non-performance of the active centers of the electrodes for higher particles and smallest particles under operation at higher C rate. The cyclic votammetry of half-cells of the corresponding electrodes is shown in the following figure.

In the electrochemistry analysis it is underlined the stable performance of the current and potential during cycling of the electrode ZnOs1 while the other electrodes revealed perturbations of current due to the potential variations that differed cycle upon cycle.

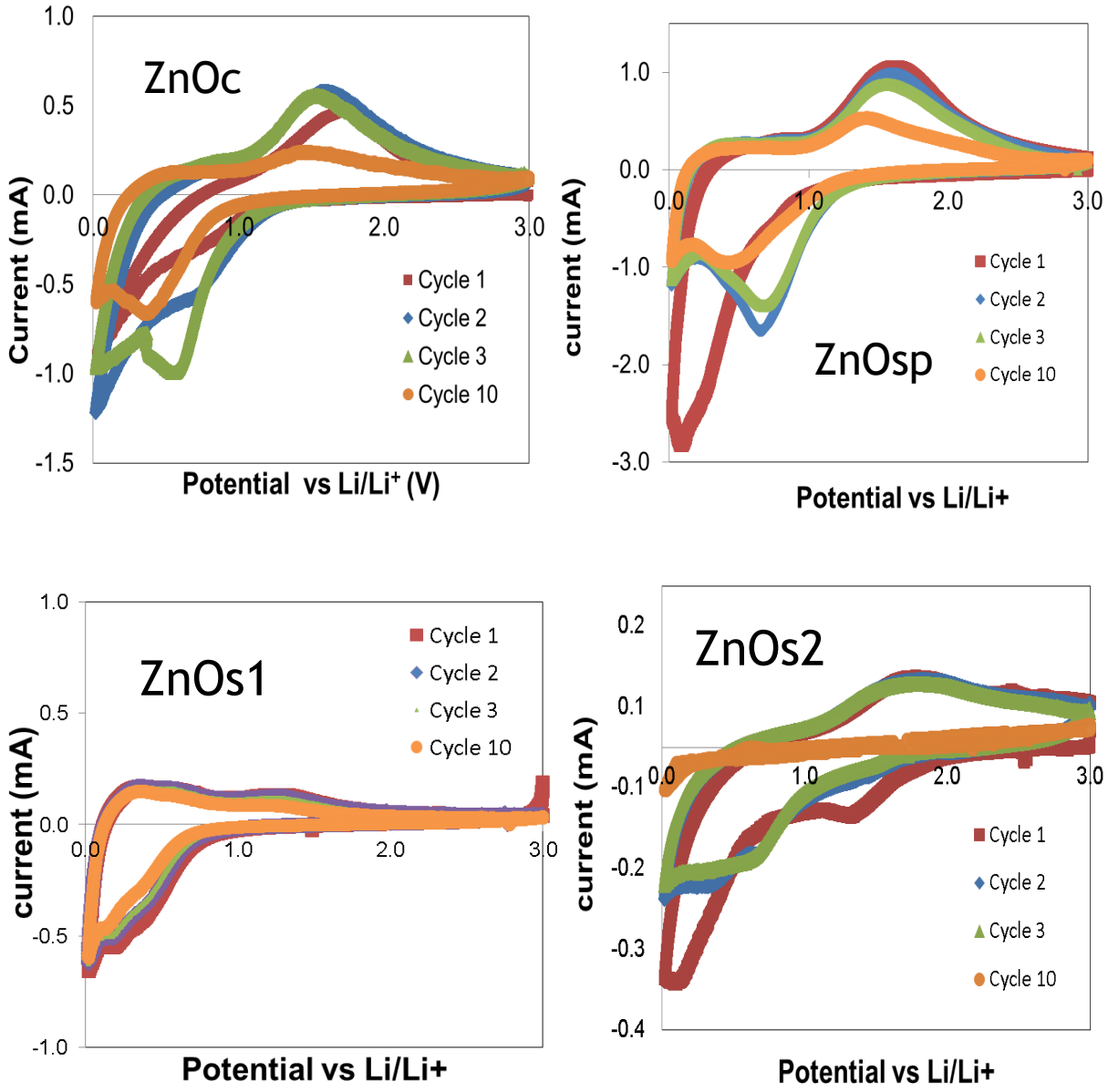

Figure 19 – Cyclic voltammetry of the electrodes ZnOc, ZnoSp, ZnOs1 and $ZnOs_2$ tested in the Basytec® software in the potential range from 0.02 V to 3.1 V with slope of 0.3 $mV.s^{-1}$ in both down and up rampage.

ZnOs1 revealed Coulombic efficiency stable (c.a. 100 %) during cycling. The milling time of the electrode fabrication was found to be suitable to produce particles in plank shape which in the

first cylces are at the beginning of the pulverization and therefore it takes more cycles for the formation of smaller particles and capacity fading.

At the 20^{th} the reversible capacity is near 300 mAh g^{-1} but it is increased due to the formation of smaller particles resulting from pulverization of the planks. The reversible capacities reaches a value c.a. 750 mAh g^{-1} at the 35^{th} cycle. At the end of 63^{th} cycle the reversible capacity is 439 mAh g^{-1} revealing that the electrode with the smallest particle size (lowest milling time) shows high durability and cyclability.

5 Conclusions

The fabrication of the of ZnO nanocomposites and their comparison with the commercial commercial active material was achieved through mechanical milling method. The half-cell preparation allowed the electrochemical testing under observation of milling time and pressure effects on the electrodes. The study and enhancement of capacity through reaction mechanism was related and complete with the structural and phase analysis.

The electrode ZnOsp had nano-size particles and higher irreversible capacity than ZnOc. Both electrodes had the same mixing time. ZnOc had capacity fading to zero in the first cycles due to the lower surface area to contact with the lithium ions. ZnOsp had capacity fading to zero after the first cycle due particle agglomeration, the loss of contact area between the electrode and the lithium-ions and increase of resistance. Micro-particles and the finest nano-particles lead to fast capacity fading, decrease of cyclability and durability. The XRD analysis revealed the broadening of peaks as the particle size are decrease from ZnOc to ZnOsp respectively. This is related with the hexagonal crystal structures and sizes observed in the SEM pictures of the electrodes before cycling and the cracks after cycling.

ZnOs1 had the lowest milling time which corresponded to planks particles that after the first cycle begin to pulverize into smaller particles.

The corresponding nano-size was the suitable to obtain the highest discharge capacity and lowest capacity fading of the synthetized electrodes. ZnOs3 and ZnOsp did not reveal results during cycling due to the high milling times and particle agglomeration due to the highest surface area that resulted in high contact resistance between electrode, active material and lithium ions.

As it is shown in figure 20, as the milling time increases, the particles become smaller and at a certain nano-size they tend to form agglomerates due to the electrostatic forces and van der wall forces of the dipole-dipole interactions of the tiny particles. For even higher milling times, the agglomerates form crystals wich does not allow complete dealloying where the lithium-ions stay into the anode leading to electrode breakdown.

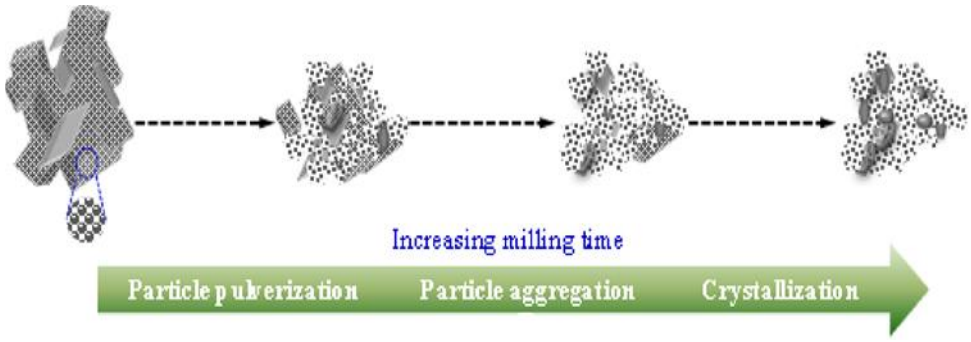

Figure 20- Influence of milling time in the particle size

There is an optimum milling time in which the electrodes synthetiyed had the plank structure in its particles and corresponds to the lowest capacity fading during cycling.

Pressing enhances the irreversible capacity of the electrodes. For the electrodes synthetized it revealed discharge capacities higher than 987 mAh g^{-1}. The procedure of pressing increases the electrode density, in the same volume there is higher contact with the lithioum ions. This fact along with the lower milling time results in more 100 mAh g^{-1} of irreversible capacity for the synthetized electrodes. At the same C rate (0.05 C rate) the electrode ZnOs2 revelead the highest discharge capacity, followed by the electrode ZnOc and ZnOsp. During cycling the capacity of ZnOsp was stable and near 300 mAh g^{-1} while the ZnOc had the highest capacity fading of all electrodes. Pressing allows less capacity fading during the first cycles.

The synthetized electrodes were contamined with Fe_xO_y although ZnOs1 had the lowest contamination due to the the lowest milling time. It is important to utilize a ceramic vessel and ceramic stainless steel bowls for the milling instead of the staineless steel materials.

ZnOs1 has the highest discharge capacity 1080 mAh g^{-1} and slow reversible capacity fading during cycling at 0.2 C rate. At the 63th cycle reveled 439 mAh g^{-1} of discharge capacity. The Coulombic efficiency during cycling was stable and near 100 %. The plank shape of the nano-particles corresponded to the suitable shape for higher capacities, higher cyclability and durability.

5.1 Suggestions for the future

ZnO is easy to synthetize through mechanical milling and it shows higher capacities than the ZnOc and ZnOsp. In this work there was contamination with Fe_xO_y which is a metal oxide along with ZnO that could reveal higher capacities for the higher amounts of this impurity present in the electrodes.

The electrodes ZnOs2 and ZnOs3 which had higher milling times than ZnOs1 and more contamination with Fe_xO_y, revealed lower capacities than the electrode ZnOs1. This allow to conclude that electrode composites alone are not the major factor in the enhancement of capacity. The synthesis of metal oxides with nano-size particles and new architectures allows higher capacities. Testing electrodes synthetized with suitable and known ratios of Fe_xO_y with ZnO may increase the conductivity and capacity due to the electrochemical proprieties of iron as a metal transition.

The growth of planks and other nano-structures (nano-wires, nano-tubes, nano-rods, flower-like) for active materials in electrodes allow higher surface contact and conductivity although it is necessary to control the size and the distribution of particles and side reactions with the electrolyte.

Fabrication of ZnO composites and zeolites promisse improve capacities though the elements added can be expensive and the techniques utilized in synthesis need higher finance investment due to the complexity of the synthesis.

The solution lies in a profound knowledge in material science, performing experimental works and testing on materials in order to find the best conditions of the anode synthesis for lithium-ion batteries, therefore there must exist more finantial investment in these areas for more advances.

This is fundamental in a world where the demand of the high capacity batteries for EV, EHV and other electric mobile systems is increasing as the population growths. The utilization and application of new high capacity anodes in lithium-ion batteries can revolutionize the mobile electric systems in the world. It provides a solution for the CO_2 emssions of the fossil fuels and it sets an attractive economical market based on electrodes investigation that never ceases to improve and discover.

References

[1] J.-M. Tarascon and M. Armand, “Issues and challenges facing rechargeable lithium batteries,” *Nature*, vol. 414, no. November, Montreal, pp. 359–367, 2001.

[2] Y. Zhang and C.-Y. Wang, “Cycle-Life Characterization of Automotive Lithium-Ion Batteries with LiNiO[sub 2] Cathode,” *J. Electrochem. Soc.*, vol. 156, no. 7, p. A527, 2009.

[3] J. K. Kaiyuan Yang, Kevin P. McGrath, Naveen Agarwal, “Lithiated quaternary composite oxides, especially of manganese, nickel, cobalt and aluminum where one of the four is present at levels of over 70 mol percent,” US 10/456,106, 2007.

[4] S. Woo, M. T. Mcdowell, L. A. Berla, W. D. Nix, and Y. Cui, “Fracture of crystalline silicon nanopillars during electrochemical lithium insertion,” pp. 1–6, 2012.

[5] H. Wu and Y. Cui, “Designing nanostructured Si anodes for high energy lithium ion batteries,” *Nano Today*, vol. 7, no. 5, pp. 414–429, Oct. 2012.

[6] S. S. Zhang, “Liquid electrolyte lithium/sulfur battery: Fundamental chemistry, problems, and solutions,” *J. Power Sources*, vol. 231, pp. 153–162, Jun. 2013.

[7] N. Imanishi and O. Yamamoto, “Rechargeable lithium – air batteries : characteristics and prospects,” *Biochem. Pharmacol.*, vol. 17, no. 1, pp. 24–30, 2014.

[8] T. M. Yoshio Idota, Masayuki Mishima, Yukio Miyaki, Tadahiko Kubota, “Nichtwässriger Akkumulator,” EP19940116643, 1995.

[9] H. Li, X. Huang, and L. Chen, “Anodes based on oxide materials for lithium rechargeable batteries 1,” vol. 123, no. October 1998, pp. 189–197, 1999.

[10] D. Fang, L. Li, W. Xu, G. Li, Z. Luo, Y. Zhou, J. Xu, and C. Xiong, “Hollow SnO 2 -ZnO hybrid nanofibers as anode materials for lithium-ion battery,” *Mater. Res. Express*, vol. 1, no. 2, p. 025012, Apr. 2014.

[11] H. Usui, T. Kono, and H. Sakaguchi, “Novel Composite Thick-Film Electrodes Consisted of Zinc Oxide and Silicon for Lithium-Ion Battery Anode,” vol. 7, pp. 4322–4334, 2012.

[12] F. Xia, S. B. Kim, H. Cheng, J. M. Lee, T. Song, Y. Huang, J. a Rogers, U. Paik, and W. Il Park, “Facile synthesis of free-standing silicon membranes with three-dimensional nanoarchitecture for anodes of lithium ion batteries.,” *Nano Lett.*, vol. 13, no. 7, pp. 3340–6, Jul. 2013.

[13] A. Mendes, “Course: Energias Renováveis I,” in *Energias Renováveis 1 - Céliulas de Combustível, Células Fotovoltaicas, Células Fotoeletroquímicas, Eletrólise e Baterias*, Faculty of Engineering of University of Porto, Master’s Degree in Chemical Engineering, 2013, pp. 19 –151.

[14] W. Schindler, *Fuel Cells in Energy Technology - Part 4*, no. 4. Technische Universität München, Department of Physics, 2014, pp. 1 – 43.

[15] D. rer. nat. N. Wagner, “Deutsches Zemtrum Für Lauft und Rauzmfahrt (DLR),” 2014. [Online]. Available: http://www.dlr.de/tt/en/desktopdefault.aspx/tabid-7197/.

[16] “Zinc Oxide Applications.” [Online]. Available: http://www.zinc.org/info/zinc_oxide_applications. [Accessed: 15-Jan-2015].

[17] Y. Chin, R. Dagle, J. Hu, A. C. Dohnalkova, and Y. Wang, “Steam reforming of methanol over highly active Pd / ZnO catalyst,” vol. 77, pp. 79–88, 2002.

[18] Y. Yang, J. Ma, and F. Wu, “Production of hydrogen by steam reforming of ethanol over a Ni/ZnO catalyst,” *Int. J. Hydrogen Energy*, vol. 31, no. 7, pp. 877–882, Jun. 2006.

[19] W. Xie and X. Huang, “Synthesis of Biodiesel from Soybean Oil using Heterogeneous KF/ZnO Catalyst,” *Catal. Letters*, vol. 107, no. 1–2, pp. 53–59, Feb. 2006.

[20] W.-J. Huang, G.-C. Fang, and C.-C. Wang, “A nanometer-ZnO catalyst to enhance the ozonation of 2,4,6-trichlorophenol in water,” *Colloids Surfaces A Physicochem. Eng. Asp.*, vol. 260, no. 1–3, pp. 45–51, Jun. 2005.

[21] G. Amin, “White LEDs Printed on Paper—A Doctoral Thesis—Part I.” [Online]. Available: http://www.edn.com/Home/PrintView?contentItemId=4391796. [Accessed: 11-Mar-2015].

[22] U. Ö. Hadis Morkoc, *Zinc Oxide: Fundamentals, Materials and Device Technology*. Virginia: Wiley, 2007, pp. 3–26.

[23] A. Kołodziejczak-Radzimska and T. Jesionowski, “Zinc Oxide—From Synthesis to Application: A Review,” *Materials (Basel).*, vol. 7, no. 4, pp. 2833–2881, Apr. 2014.

[24] Z. L. Wang, “Zinc oxide nanostructures: growth, properties and applications,” *J. Phys. Condens. Matter*, vol. 16, no. 25, pp. R829–R858, Jun. 2004.

[25] M. Suchea, S. Christoulakis, K. Moschovis, N. Katsarakis, and G. Kiriakidis, “ZnO transparent thin films for gas sensor applications,” *Thin Solid Films*, vol. 515, no. 2, pp. 551–554, Oct. 2006.

[26] D. C. Look and B. Claflin, “P-type doping and devices based on ZnO,” *Phys. Status Solidi*, vol. 241, no. 3, pp. 624–630, Mar. 2004.

[27] E. Hosono, S. Fujihara, I. Honma, and H. Zhou, “The Fabrication of an Upright-Standing Zinc Oxide Nanosheet for Use in Dye-Sensitized Solar Cells,” *Adv. Mater.*, vol. 17, no. 17, pp. 2091–2094, Sep. 2005.

[28] G. D. W. Perry, Robert H., *Perry Chemical Engineers ’ Handbook*. Mac-Graw Hill, 1999.

[29] A. Vu, Y. Qian, and A. Stein, “Porous Electrode Materials for Lithium-Ion Batteries - How to Prepare Them and What Makes Them Special,” *Adv. Energy Mater.*, vol. 2, no. 9, pp. 1056–1085, Sep. 2012.

[30] Q. Xie, Y. Ma, X. Zhang, L. Wang, G. Yue, and D.-L. Peng, "ZnO/Ni/C composite hollow microspheres as anode materials for lithium ion batteries," *J. Alloys Compd.*, vol. 619, pp. 235–239, Jan. 2015.

[31] Y. Wang, X. Jiang, L. Yang, N. Jia, and Y. Ding, "In Situ Synthesis of C / Cu / ZnO Porous Hybrids as Anode Materials for Lithium Ion Batteries," vol. c, no. iii, 2014.

[32] Y. Zhao, G. Chen, and Y. Wang, "Facile Synthesis of Graphene/ZnO Composite as an Anode with Enhanced Performance for Lithium Ion Batteries," *J. Nanomater.*, vol. 2014, pp. 1–6, 2014.

[33] X. Zheng, Y. Li, Y. Xu, Z. Hong, and M. Wei, "Metal–organic frameworks: Promising materials for enhancing electrochemical properties of nanostructured Zn2SnO4 anode in Li-ion batteries," *CrystEngComm*, vol. 14, no. 6, p. 2112, 2012.

[34] F. Belliard and J. T. S. Irvine, "Electrochemical performance of ball-milled ZnO ± SnO 2 systems as anodes in lithium-ion battery," vol. 98, pp. 219–222, 2001.

[35] D. Bresser, F. Mueller, M. Fiedler, S. Krueger, R. Kloepsch, D. Baither, M. Winter, E. Paillard, and S. Passerini, "Transition-Metal-Doped Zinc Oxide Nanoparticles as a New Lithium-Ion Anode Material," *Chem. Mater.*, vol. 25, no. 24, pp. 4977–4985, Dec. 2013.

[36] M. Yu, A. Wang, Y. Wang, C. Li, and G. Shi, "An alumina stabilized ZnO-graphene anode for lithium ion batteries via atomic layer deposition.," *Nanoscale*, vol. 6, no. 19, pp. 11419–24, Sep. 2014.

[37] M. Ahmad, S. Yingying, A. Nisar, H. Sun, W. Shen, M. Wei, and J. Zhu, "Synthesis of hierarchical flower-like ZnO nanostructures and their functionalization by Au nanoparticles for improved photocatalytic and high performance Li-ion battery anodes," *J. Mater. Chem.*, vol. 21, no. 21, p. 7723, 2011.

[38] ab H. Z. and M. W. Cheng Zheng, ab Lingxing Zeng, ab Meili Wang, "Synthesis of hierarchical ZnV2O4 microspheres and its electrochemical properties," *CrystEngComm*, vol. 16, no. 44, pp. 10309–10313, 2014.

[39] E. Hosono, S. Fujihara, T. Kimura, and H. Imai, "Growth of layered basic zinc acetate in methanolic solutions and its pyrolytic transformation into porous zinc oxide films.," *J. Colloid Interface Sci.*, vol. 272, no. 2, pp. 391–8, Apr. 2004.

[40] F. Zou, X. Hu, Z. Li, L. Qie, C. Hu, R. Zeng, Y. Jiang, and Y. Huang, "MOF-Derived Porous ZnO/ZnFe2 O4 /C Octahedra with Hollow Interiors for High-Rate Lithium-Ion Batteries.," *Adv. Mater.*, vol. 26, no. 38, pp. 6622–8, Oct. 2014.

[41] H. Yue, Z. Shi, Q. Wang, Z. Cao, H. Dong, Y. Qiao, Y. Yin, and S. Yang, "MOF-derived cobalt-doped ZnO@C composites as a high-performance anode material for lithium-ion batteries.," *ACS Appl. Mater. Interfaces*, vol. 6, no. 19, pp. 17067–74, Oct. 2014.

[42] X. H. Huang, J. B. Wu, Y. Lin, and R. Q. Guo, "ZnO Microrod Arrays Grown on Copper Substrates as Anode Materials for Lithium Ion Batteries," vol. c, pp. 6611–6621, 2012.

[43] W. Song, J. Xie, S. Liu, Y. Zheng, G. Cao, and T. Zhu, "Graphene Decorated with ZnO Nanocrystals with Improved Electrochemical Properties Prepared by a Facile In Situ Hydrothermal Route," vol. c, pp. 2164–2174, 2012.

[44] C.-T. Hsieh, C.-Y. Lin, Y.-F. Chen, and J.-S. Lin, "Synthesis of ZnO@Graphene composites as anode materials for lithium ion batteries," *Electrochim. Acta*, vol. 111, pp. 359–365, Nov. 2013.

[45] X. Shen, D. Mu, S. Chen, B. Wu, and F. Wu, "Enhanced electrochemical performance of ZnO-loaded/porous carbon composite as anode materials for lithium ion batteries.," *ACS Appl. Mater. Interfaces*, vol. 5, no. 8, pp. 3118–25, Apr. 2013.

[46] S. M. Abbas, S. T. Hussain, S. Ali, N. Ahmad, N. Ali, and S. Abbas, "Structure and electrochemical performance of ZnO/CNT composite as anode material for lithium-ion batteries," *J. Mater. Sci.*, vol. 48, no. 16, pp. 5429–5436, Mar. 2013.

[47] P. Balaz, "High-Energy Milling," in *Mechanochemistry in Nanoscience and Minerals Engineering*, 2008.

[48] A. K. Bharathi, "Analysis of the thermal proprieties of zinc oxide using the reaxFF reactive force field," 2010.

[49] L. C. Damonte, L. a. Mendoza Zélis, B. Marí Soucase, and M. a. Hernández Fenollosa, "Nanoparticles of ZnO obtained by mechanical milling," *Powder Technol.*, vol. 148, no. 1, pp. 15–19, Oct. 2004.

[50] X. H. Huang, X. H. Xia, Y. F. Yuan, and F. Zhou, "Porous ZnO nanosheets grown on copper substrates as anodes for lithium ion batteries," *Electrochim. Acta*, vol. 56, no. 14, pp. 4960–4965, May 2011.

Annex 1 Synthesis Methods of Zinc Oxide

Method	Precursors	Synthesis conditions	Properties and applications
Mechanochemical process	$ZnCl_2$, Na_2CO_3, NaCl	calcination: 2 h, 600 °C 400–800 °C 400 °C 0.5 h 300–450 °C	hexagonal structure; particles diameter: 21–25 nm hexagonal structure; particles diameter: 18–35 nm regular shape of particles; diameter ~27 nm, *BET*: 47 m^2/g particles diameter: 27–56 nm particles diameter: ~51 nm, *BET*: 23 m^2/g
Precipitation process	$Zn(CH_3COO)_2$, and KOH as a water solutions	temperature of process: 20–80 °C; drying: 120 °C	particles diameter: 160–500 nm, *BET*: 4–16 m^2/g
	$Zn(CH_3COO)_2$, $(NH_4)_2CO_3$, PEG10000 as a water solutions	drying: 12 h, 100 °C; calcination: 3 h, 450 °C	zincite structure; spherical particles (*D* ~ 30 nm); application: as a photocatlyst in photocatalytic degradation
	$Zn(NO_3)_2$	calcination: 2 h, 600 °C; aging: 240 h, 320 °C	wurtize structure; particles diameter: 50 nm; application: as a gas sensor
	$Zn(NO_3)_2$, NaOH	synthesis: 2 h; drying: 2 h, 100 °C	particles of spherical size of around 40 nm
	$ZnSO_4$, NH_4HCO_3, ethanol	drying: overnight, 100 °C; calcination: 300–500 °C	wurtize structure; crystallite size 9–20 nm; particle size *D*: ~12 nm, *BET*: 30–74 m^2/g
	$Zn(CH_3COO)_2$, NH_3 aq.	precipitation temperature: 85 °C; drying: 10 h, 60 °C	hexagonal structure, shape of rods, flower-like particles: *L*: 150 nm, *D*: 200 nm
	$ZnSO_4$, NH_4OH, NH_4HCO_3	reaction: 30 min, 60 °C; drying: 12 h, 100 °C; calcination: 2 h, 400 °C	hexagonal structure, flake-like morphology (*D*: 0.1–1 μm, *L*: 60 nm)
	microsized ZnO powder, NH_4HCO_3	reaction: ~2 h, 25 °C; drying: 80 °C; calcination:1 h, 350 °C	hexagonal wurtize structure; flower-like and rod-like shape (*D*: 15–25 nm, *BET*: 50–70 m^2/g)
	$Zn(CH_3COO)_2$, NaOH	reaction: 30 min, 75 °C; drying: overnight, room temperature	hexagonal structure; flower shape (*L*: >800 nm); application: antimicrobial activity
Precipitation in the presence of surfactants	$ZnCl_2$, NH_4OH, CTAB	aging: 96 h, ambient temperature, calcination: 2 h, 500 °C	zincite structure; particles diameter: 54–60 nm, *BET* = ~17 m^2/g
	$Zn(NO_3)_2$, NaOH, SDS, TEA (triethanolamine)	precipitation: 50–55 min, 101 °C	wurtize structure, shape of rod-like (*L*: 3.6 μm, *D*: 400–500 nm) shape of nut-like and rice-like, size: 1.2–1.5 μm
Mechanochemical process	$ZnCl_2$, Na_2CO_3, NaCl	calcination: 2 h, 600 °C 400–800 °C 400 °C 0.5 h 300–450 °C	hexagonal structure; particles diameter: 21–25 nm hexagonal structure; particles diameter: 18–35 nm regular shape of particles; diameter ~27 nm, *BET*: 47 m^2/g particles diameter: 27–56 nm particles diameter: ~51 nm, *BET*: 23 m^2/g
Precipitation process	$Zn(CH_3COO)_2$, and KOH as a water solutions	temperature of process: 20–80 °C; drying: 120 °C	particles diameter: 160–500 nm, *BET*: 4–16 m^2/g
	$Zn(CH_3COO)_2$, $(NH_4)_2CO_3$, PEG10000 as a water solutions	drying: 12 h, 100 °C; calcination: 3 h, 450 °C	zincite structure; spherical particles (*D* ~ 30 nm); application: as a photocatlyst in photocatalytic degradation
	$Zn(NO_3)_2$	calcination: 2 h, 600 °C; aging: 240 h, 320 °C	wurtize structure; particles diameter: 50 nm; application: as a gas sensor
	$Zn(NO_3)_2$, NaOH	synthesis: 2 h; drying: 2 h, 100 °C	particles of spherical size of around 40 nm
	$ZnSO_4$, NH_4HCO_3, ethanol	drying: overnight, 100 °C; calcination: 300–500 °C	wurtize structure; crystallite size 9–20 nm; particle size *D*: ~12 nm, *BET*: 30–74 m^2/g
	$Zn(CH_3COO)_2$, NH_3 aq.	precipitation temperature: 85 °C; drying: 10 h, 60 °C	hexagonal structure, shape of rods, flower-like particles: *L*: 150 nm, *D*: 200 nm
	$ZnSO_4$, NH_4OH, NH_4HCO_3	reaction: 30 min, 60 °C; drying: 12 h, 100 °C; calcination: 2 h, 400 °C	hexagonal structure, flake-like morphology (*D*: 0.1–1 μm, *L*: 60 nm)
	microsized ZnO powder, NH_4HCO_3	reaction: ~2 h, 25 °C; drying: 80 °C; calcination:1 h, 350 °C	hexagonal wurtize structure; flower-like and rod-like shape (*D*: 15–25 nm, *BET*: 50–70 m^2/g)
	$Zn(CH_3COO)_2$, NaOH	reaction: 30 min, 75 °C; drying: overnight, room temperature	hexagonal structure; flower shape (*L*: >800 nm); application: antimicrobial activity
Precipitation in the presence of surfactants	$ZnCl_2$, NH_4OH, CTAB	aging: 96 h, ambient temperature, calcination: 2 h, 500 °C	zincite structure; particles diameter: 54–60 nm, *BET* = ~17 m^2/g
	$Zn(NO_3)_2$, NaOH, SDS, TEA (triethanolamine)	precipitation: 50–55 min, 101 °C	wurtize structure, shape of rod-like (*L*: 3.6 μm, *D*: 400–500 nm) shape of nut-like and rice-like, size: 1.2–1.5 μm

Microemulsion	$Zn(NO_3)_2$, oxalic acid, isooctane, benzene, ethanol, diethyl ether, chloroform, acetone, methanol, Aerosol OT	reaction: 1 h; calcination: 3 h, 300 °C	equivalent spherical diameter: 11.7–12.9 nm, *BET*: 82–91 m^2/g; grain size: 11–13 μm
	$Zn(CH_3COO)_2$, Aerosol OT, glycerol, $C_{20}H_{37}NaO_7S$, n-heptane, NaOH, methanol, chloroform	reaction: 24 h, 60–70 °C; drying: 1 h, 100 °C; calcination: 3 h, 300–500 °C	hexagonal wurtize structure, spherical shape (15–24 nm), rods shape (*L*: 66–72 nm, *D*: 21–28 nm)
	$ZnCl_2$, $Zn(CH_3COO)_2$, heptane, BTME (1,2-trimethoxysilyl)ethane, TMOS (tetramethoxysilane), methanol, Aerosol OT, NaOH	reaction: 2–3 h, room temperature or 40 °C; drying: under vacuum overnight; calcinations: 24 h, 700 °C	hexagonal structure, uniformly dispersed small particles, size of particles ~10 nm
Other method	$Zn(CH_3COO)_2$	thermal decomposition: 350–800 °C	uniform size of particles 20–30 nm
	$Zn(NO_3)_2$, deionized water, HMT (hexamethylenetetramine)	ultrasonic irradiation: 30 min, 80 °C; drying: 2 h, 60 °C	hexagonal wurtize structure, nanorod and nanowire shape (*L*: ~1 μm, *D*: ~160 nm); application: electronic and optoelectronic devices
	micron scale zinc metal powder	feed rate: 1 g/min; plasma power: 1 kW; O_2 flow rate: 2.5 lpm; N_2 flow rate: 12.5 lpm; reaction: 900 °C	nanowires shape (*L*: 1–30 μm, *D*: 5–50 nm) application: as hydrodesulfurization catalyst
	diethylzinc (DEZ), oxygen	helium as a carrier gas	wurtize structure; average particle size: 9 nm

Radzimska at al. Materials 2014, 7(4), 2833-2881

Annex 2 Electrode coatings and water effects

The conditons set for the ZnO sintetized and ZnO suspension were set after fabrication of the electrondes with ZnO commercial. The amount of water added (5 mL) to the preparation of the electrodes was found out to provide a flat coating and electrode homogeniety.

It was produced ZnOc1, ZnOc2 and ZnOc3. ZnOc1 and ZnOc2 electrodes with 28 ml and 10 ml of water, respectively, which led to a cupper foil with a roughness surface even at 100 nm of coating thickness. ZnOc3 had no content of water added and led to a fast drying and breaking of the cupper foil after the doctor blade coating. ZnOc4 had 5 ml of water and an improved flat surface of all the commercial electrode samples.

Annex 3 Pressing equipment

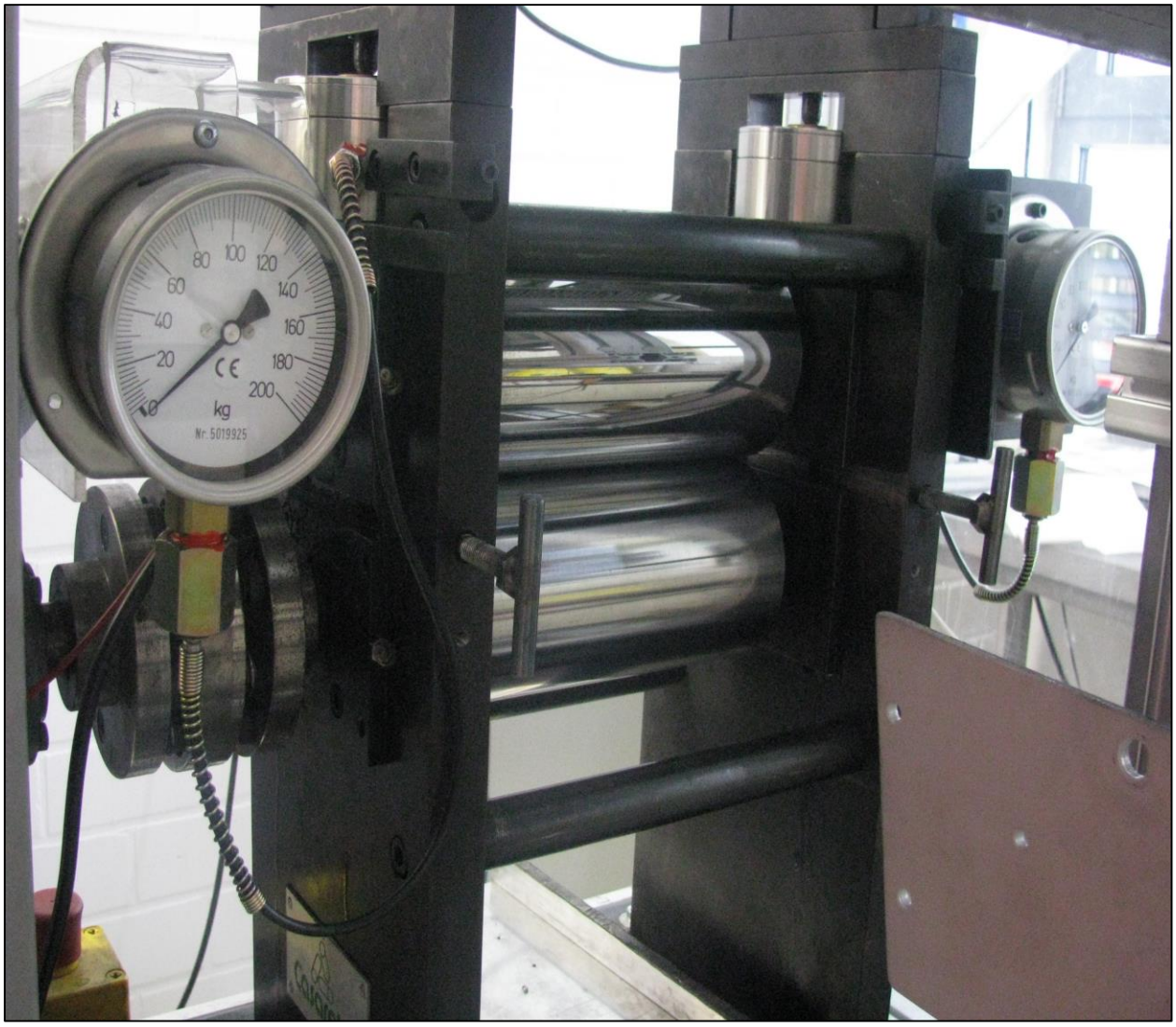

DLR -Institute of Engineering Thermodynamics self-made pressing equipment